R. & M. No. 3361

MINISTRY OF AVIATION

AERONAUTICAL RESEARCH COUNCIL
REPORTS AND MEMORANDA

Pressure-Plotting and Force Tests at Mach Numbers up to 2·8 on an Uncambered Slender Wing of $p = \frac{1}{2}$, $s/c_0 = \frac{1}{4}$ ('Handley Page Ogee')

By A. L. Courtney and A. O. Ormerod

LONDON: HER MAJESTY'S STATIONERY OFFICE
1964
PRICE £1 5s. 0d. NET

Pressure-Plotting and Force Tests at Mach Numbers up to 2·8 on an Uncambered Slender Wing of $p = \frac{1}{2}$, $s/c_0 = \frac{1}{4}$ ('Handley Page Ogee')

By A. L. COURTNEY and A. O. ORMEROD

COMMUNICATED BY THE DEPUTY CONTROLLER AIRCRAFT (RESEARCH AND DEVELOPMENT), MINISTRY OF AVIATION

*Reports and Memoranda No. 3361**
May, 1961

Summary.

Pressure-plotting and force tests have been made in the 8 ft × 8 ft Wind Tunnel, Bedford, on an uncambered slender wing of Collingbourne $p = \frac{1}{2}$ ogee planform, $s/c_0 = 0{\cdot}25$, 'Newby' area distribution, and varying cross-section shape representing an aircraft with a central passenger cabin blending into the wing. The model is one of two designed by Messrs. Handley Page under the auspices of the Supersonic Transport Aircraft Committee.

At zero lift, the wave-drag factor K_0 is about 0·2 below the slender-theory value at all Mach numbers, due to the absence of a predicted rapid expansion towards the trailing edge, and further work on sting interference seems desirable. Apart from the difference near the trailing edge, the measured zero-lift pressures are in quite good agreement with slender or linear thin-wing theory.

At incidence, the pressure gradients are everywhere favourable behind the leading-edge vortex, and there is a large trailing-edge load which is not predicted by slender theory. The cruising centre of pressure is $0{\cdot}075c_0$ behind the low-speed aerodynamic centre at $C_L = 0{\cdot}5$. At $M = 2{\cdot}2$, K_0 is 0·72 and the lift-dependent drag factor is 1·92, giving an estimated full-scale maximum L/D of 8·3 excluding engines.

LIST OF CONTENTS

Section

* Replaces R.A.E. Tech. Note No. Aero. 2760—23 109.

Section

LIST OF TABLES

Table

LIST OF ILLUSTRATIONS

Figure

---

1. *Introduction.*

This report describes pressure-plotting and force tests made in the 8 ft × 8 ft Wind Tunnel, Royal Aircraft Establishment, Bedford, on the uncambered member of a pair of slender wings of Collingbourne $p = \frac{1}{2}$ ogee planform designed by Messrs. Handley Page Ltd.[1] under the auspices of the Supersonic Transport Aircraft Committee. The wing has overall characteristics as follows:

$$\text{L.E. shape } \frac{s(x)}{s_T} = \tfrac{1}{2}x + x^2 - \tfrac{1}{2}x^5$$

$$s_T = 0\cdot 25c_0$$

$$p = \frac{\text{wing area}}{2s_Tc_0} = 0\cdot 5$$

$$\text{Aspect ratio } A = 1$$

$$\text{Area distribution } S(x) = 0\cdot 0515\,(x^2 - x^3)c_0^{\,2} \text{ ('Newby')}$$

$$\text{Volume coefficient } \tau = \frac{\text{Volume}}{(\text{wing area})^{3/2}} = 0\cdot 0343$$

and with varying cross-section shapes, as shown in Fig. 1, representing a possible design with a central passenger cabin blending smoothly into the wing cross-section.

Several factors entered into the choice of a configuration of this kind for wind-tunnel testing. When the tests were planned in 1958, some experimental evidence existed on delta and gothic planforms with simple rhombic or parabolic cross-sections, which had been tested mainly from the viewpoint of providing basic comparisons with theory. It seemed likely, however, that a practical aircraft would differ in several respects from the simple models that had so far been tested, e.g.:

(i) it would have a more complicated cross-section shape with a thickened centre section for more efficient volume utilization,

(ii) it would probably have a planform with streamwise tips, but with a lower value of 'p' than the $0 \cdot 67$ of the gothic wing, from considerations of balance and lift/drag ratio,

(iii) it would have streamwise and spanwise camber to provide trim under cruising conditions whilst maintaining low lift-dependent drag and good flow development and lift for take-off and landing.

A detailed study[2] undertaken by Messrs. Handley Page examined these and other factors in the context of a practical aircraft able to accommodate its passengers and fuel, capable of being balanced, and with acceptable cruising efficiency and airfield performance, and this led to the proposals by Clark in Ref. 1 for uncambered and cambered models of $p = 0 \cdot 5$ ogee planform, Newby area distribution and varying cross-section shape.

Since one aim of the tests was to investigate the adequacy of slender-wing design methods applied to more-complicated shapes than hitherto, it was decided that both models should be extensively pressure-plotted as well as force tested. The uncambered model, in addition to providing a datum for the camber tests, would show the effects on pressure distribution of the varying cross-section shape of a practical aircraft, and the cambered model would give information on the camber design methods[1,3,4] and show up any regions of adverse pressure gradient or flow separation due to camber.

This report gives, for the uncambered wing, the overall lift, drag and pitching-moment results from balance tests at Mach numbers from $0 \cdot 3$ to $2 \cdot 8$, together with a complete set of tabulated pressure-plotting results. The balance tests have been analysed to give zero-lift and lift-dependent drag factors, lift-curve slopes and centres of pressure. Some of the pressure-plotting results have been integrated to give zero-lift drag and streamwise and spanwise distributions of lift, and comparisons are made between the experimental pressure and load distributions and the predictions of slender and/or linear thin-wing theory.

2. *Details of Model and Tests.*

2.1. *Model.*

The main design parameters have been given in Section 1. Further details are given in Figs. 1 to 3 showing the general arrangement of the model, pressure-plotting orifices and sting shrouds, and the chordwise and spanwise section shapes. The spanwise section shapes can be expressed analytically; details are given in Ref. 1.

The model was constructed by the Aircraft Research Association, Bedford, and was made of steel with pressure-plotting tubes laid in surface slots filled with Araldite. Root chord was 60 inches and span 30 inches. The main pressure-plotting stations were on the centre-line and at $0 \cdot 125$, $0 \cdot 33$, $0 \cdot 55$ and $0 \cdot 80$ of the semi-span. These were on one surface only, the model being tested at positive and negative incidences to give upper-surface and lower-surface pressure distributions.

The model was sting-supported on its centre-line, and where the sting broke through the wing surface at the rear the model ordinates were distorted by the addition of a sting shroud covering the affected region. For the force tests the sting shroud consisted of a circular cylinder of $3 \cdot 35$ inches diameter, Fig. 1; for the main pressure-plotting tests a smaller sting was used and the shroud was an elliptic cylinder with axes of $2 \cdot 9$ inches and $2 \cdot 6$ inches normal to and parallel to the wing chord plane respectively.

2.2. *Tests.*

The main balance and pressure-plotting tests were made at a Reynolds number of 2×10^6 per foot, giving a Reynolds number of 10^7 on root chord; in addition, some tests were made at $M = 2 \cdot 0$ with the Reynolds number reduced to 10^6 per foot.

In the balance tests, results were obtained at Mach numbers of $0 \cdot 3$, $1 \cdot 4$, $1 \cdot 6$, $1 \cdot 7$, $1 \cdot 8$, $2 \cdot 0$, $2 \cdot 2$, $2 \cdot 4$, $2 \cdot 6$ and $2 \cdot 8$, the incidence range (positive and negative) being generally $0°$ to $12°$ in steps of $0 \cdot 5°$ or $1°$. For these tests 60-grade carborundum grit was applied in a $0 \cdot 5$ inch band close to the leading edge on upper and lower surfaces in order to fix transition. Azobenzene sublimation tests at a Mach number of $2 \cdot 4$ showed that this was effective in producing transition at the test Reynolds number of 2×10^6 per foot.

In the pressure-plotting tests, results were obtained at Mach numbers of $1 \cdot 4$, $1 \cdot 8$, $2 \cdot 0$, $2 \cdot 4$ and $2 \cdot 8$. With free transition and the small pressure-plotting sting shroud the incidences tested were 0, 1, 2, 3, 4, 6, 8 and 12 degrees (positive and negative). Some tests were also made with fixed transition and the larger sting shroud of the forces tests; these covered the same range of Mach numbers but were restricted to incidences of 0, 2, 4 and 6 degrees.

Oil-flow studies of the flow close to the upper surface were made at an incidence of 6 degrees at Mach numbers of $1 \cdot 4$, $2 \cdot 0$, $2 \cdot 4$ and $2 \cdot 8$, using a mixture of titanium oxide in oil.

3. *Reduction and Presentation of Results.*

3.1. *Balance Tests.*

The overall lift, drag and pitching-moment results from the balance tests are given with some analysis in Figs. 4 to 11. In the C_L vs. α curves of Fig. 4 the incidence has been corrected for sting deflection under load but not for possible downwash or curvature of the working-section flow. As can be seen in Figs. 4 to 7, the lift and pitching-moment curves do not pass exactly through the origin, and additional balance tests with the model (and axes) inverted give lift curves displaced on the opposite side of the origin, indicating some downwash or curvature in the tunnel flow, Fig. 5. The maximum error in incidence is less than $0 \cdot 1°$. The effects of inverting the model on pitching moments are shown in Fig. 7, and here it can be seen that the mean values of $C_{m\,0}$ (based on $\bar{c}$) as between model upright and inverted are not zero but vary smoothly from about $-0 \cdot 0004$ at $M = 1 \cdot 4$ to $-0 \cdot 0002$ at $M = 2 \cdot 8$; this could be due to balance errors or to slight asymmetry in the model. The maximum measured difference in $C_{m\,0}$ between model upright and inverted is $0 \cdot 0012$ at $M = 1 \cdot 6$, representing, if genuine, a tunnel flow curvature equivalent to a $\Delta C_{m\,0}$ of $0 \cdot 0006$ at this Mach number. Tunnel flow effects are also apparent in Fig. 11 giving the overall lift-dependent drag factor

$$K = \frac{\pi A(C_D - C_{D\,0})}{C_L^{\,2}} \qquad (1)$$

which is different for positive and negative incidences. It is assumed that the true value of K is given by the mean value for positive and negative incidences; the lower part of Fig. 11 shows that this gives very good agreement with the mean experimental curve of Ref. 7.

These departures from complete model and tunnel symmetry cause no difficulty in the interpretation and analysis of the present results for the symmetrical wing, and it is not proposed to pursue them further at this stage. Attention is drawn to them mainly because of their relevance in the testing and analysis of cambered wings where extra care is obviously needed; the apparent ΔC_{m0} of $0 \cdot 0006$ at $M = 1 \cdot 6$, for instance, represents about 15% of the design C_{m0} for a cambered version of the present wing.

Pitching-moment coefficients are based on the aerodynamic mean chord $\bar{c}$ ($= 0 \cdot 62 c_0$) and are quoted about an arbitrarily chosen axis at $0 \cdot 5\bar{c}$ ($0 \cdot 69 c_0$) giving roughly neutral stability.

The overall drag coefficients have been adjusted to free-stream static pressure over the sting-shroud base area, and are presented both corrected and uncorrected for sting interference in Fig. 9. The sting interference has been estimated in two parts, namely

(i) an allowance for the rearward-facing wing surface masked by the cylindrical sting shroud, and

(ii) an allowance for the pressure field of the sting shroud based on some pressure-plotting measurements with and without sting on another wing.

The estimated corrections for the balance sting are:

Mach number	1·4	1·8	2·0	2·4	2·8
(i) ΔC_D (masking)	0·00053	0·00040	0·00034	0·00029	0·00024
(ii) ΔC_D (pressure field)	0·00072	0·00052	0·00045	0·00034	0·00029
Total ΔC_D	0·00125	0·00092	0·00079	0·00063	0·00053

The overall corrections are quite large, amounting to about one-third of the zero-lift wave drag, and emphasize the need for more information on sting interference effects to improve the accuracy of estimation. In the present case it will be seen below that very good agreement is obtained between the integrated pressure drag and the wave drag derived from the balance tests using the above corrections and an estimated skin-friction drag, but in view of other uncertainties this cannot be taken as establishing the accuracy of the assumed sting corrections.

In Fig. 9, comparing the zero-lift wave drag derived from the balance tests with that obtained by integrating the measured pressure distributions, the sting correction for the pressure-plotting results consists only of the pressure-field term, the masking term being avoided by extrapolating the measured pressures to the centre-line as though the sting shroud were absent. Because of this, and the smaller size of the pressure-plotting sting, the corrections to the pressure-plotting results are only about half those given above for the balance tests.

3.2. *Pressure-Plotting Tests.*

The measured values of $10^3 C_p$ for all test Mach numbers and incidences are given in Tables 1 to 3. Table 1 gives the results with transition free and the small sting shroud, at $R = 2 \times 10^6$ per foot; Table 2 shows the effect of reducing R to 1×10^6 per foot at $M = 2$; and Table 3 gives the results with transition fixed and the large sting shroud, at $R = 2 \times 10^6$ per foot. The results are tabulated against x/c_0 at various spanwise positions, where x is the distance from the wing apex and c_0 is the centre-line chord. Positive and negative incidences, respectively, refer to upper-surface and lower-surface pressures. The incidences are corrected for sting deflection under load, but not for tunnel flow effects.

A graphical presentation of some of the basic pressure-plotting data is given in Figs. 12 to 15 where C_p is plotted against x/c_0 for the various pressure-plotting stations. In these figures the incidences are corrected for sting deflection but not for tunnel flow effects. In Figs. 16 to 21, however, involving loads per unit incidence, small corrections have been applied to the incidence values using Fig. 5. The effects on the basic pressure distributions are also small, as can be seen from Fig. 13 showing the effect at one pressure-plotting station of inverting the model at various Mach numbers.

Fig. 13 includes, of course, experimental inaccuracies as well as the direct effects of inverting the model. The accuracy of the capsule manometers used in these tests corresponds to a random scatter of about $\pm\ 0 \cdot 004$ in C_p on individual pressure readings. In addition, there is evidence of an effective zero error increasing or decreasing the general pressure level for any one scan of the manometers, i.e. at one incidence setting. This is due partly to variations in tunnel stagnation pressure, which was used as the common reference or datum pressure on one side of all the manometers, and partly, it is thought, to condensation in the working section. The results suggest a possible inaccuracy of about $\pm 0 \cdot 005$ in C_p due to this, on any set of readings at one incidence*. No attempt has been made here to correct the basic data for this type of error, but in deriving the load distributions of Figs. 16 to 21 a watch has been kept for obvious discontinuities arising from this cause, and appropriate corrections included, making use also of comparisons between the integrated loadings and the balance measurements.

3.3. *Flow Visualization.*

Photographs of oil flow on the upper surface at $\alpha = 6 \cdot 4°$ and various Mach numbers are given in Fig. 23. In these pictures transition is fixed on the port wing and free on the starboard wing; this does not seem to have produced any significant differences in the flow pattern at the test incidence. The difference in texture and flow development on the two sides is due to the use of different oils, castor oil on the starboard wing and the more usual mineral oil on the port wing; the castor oil gave the final well-scrubbed picture more quickly but remained sufficiently fluid to give a new pattern if conditions were altered. In this connection it should be noted that the $M = 2 \cdot 4$ picture was produced immediately after the $M = 2 \cdot 8$ picture, without a fresh application of oil; the traces of the $M = 2 \cdot 8$ pattern which remain, particularly on the port wing, should therefore be ignored. It should also be remembered that there is considerable distortion in perspective in Fig. 23 due to the off-centre camera position.

4. *Overall Force Results.*

4.1. *Lift.*

Lift curves for Mach numbers of $0 \cdot 3$ to $2 \cdot 8$ are given in Fig. 4. The dashed lines represent the slope at zero incidence, and the amount of non-linear lift developed can be seen by the departure of the experimental points from these lines at high incidences. As is usually found, the non-linear

* This type of inaccuracy will be reduced in future tests by using atmospheric pressure instead of tunnel stagnation pressure as the reference pressure for the manometers.

lift contribution decreases as Mach number increases, and on this wing it is relatively small beyond $M = 2$, i.e. when $\beta s/c_0$ approaches and exceeds about $0 \cdot 5$. At low speed ($M = 0 \cdot 3$) it is given quite closely by

$$\Delta C_L = 2 \cdot 5\alpha^2 .$$

The non-linear lift contribution at a typical cruising lift coefficient of $0 \cdot 075$ can be seen from Fig. 6 giving C_L/α at $C_L = 0$ and $C_L = 0 \cdot 075$ plotted against Mach number. It amounts to about 10% at $M = 0 \cdot 3$ and $M = 1 \cdot 4$, but by $M = 2 \cdot 0$ it has fallen to only about 3%.

The zero-incidence lift slope, Fig. 6, is $1 \cdot 41$ at low Mach number, rising to about $1 \cdot 65$ transonically then falling steadily to $1 \cdot 16$ at $M = 2 \cdot 8$. The transonic value is fairly close to that given by slender-wing theory, $\pi A/2 = 1 \cdot 57$. Fig. 6 shows that at Mach numbers up to about 2 the lift slope agrees well with the linear-theory value for a cropped delta wing of the same aspect ratio and span[8]. At higher speeds, however, it falls below this value and becomes more nearly equal to that for a delta wing of the same aspect ratio[8].

4.2. *Pitching Moments.*

At low speed ($M = 0 \cdot 3$) Fig. 7 shows that C_m varies linearly with C_L up to about $C_L = 0 \cdot 25$, with a progressive reduction in stability at higher incidences. The low-speed aerodynamic centre, Fig. 8, is at $0 \cdot 639\ c_0$ at low incidences, moving forward to $0 \cdot 624 c_0$ at $C_L = 0 \cdot 5$. The aerodynamic-centre position at $C_L = 0 \cdot 5$ is about $0 \cdot 03 c_0$ further forward than the mean value suggested by an unpublished correlation by Spence in terms of planform centre of area ($0 \cdot 691 c_0$ for the present wing).

At supersonic speeds, as discussed earlier, the C_m vs. C_L curves of Fig. 7 do not pass through the origin but exhibit C_{m0} values which are generally less than $0 \cdot 0005$. In view of the nominal symmetry of the model these non-zero C_{m0} values have been ignored in calculating the centres of pressure given in Fig. 8. The effect of this is small, however, and the centres of pressure obtained simply by dividing the uncorrected C_m by C_L in the normal manner do not differ by more than about $0 \cdot 005\ c_0$ from the curve shown.

Another feature of Fig. 7 is the inflected shape of the C_m vs. C_L curves near $C_L = 0$, where there is a reduction in stability. This is exaggerated in Fig. 7 by the open C_m scale for the supersonic results; the experimental scatter appears large for the same reason. The reduction of stability is generally of the order of $0 \cdot 01\bar{c}$, except at $M = 1 \cdot 4$ where it amounts to $0 \cdot 02\bar{c}$. It has been observed on other wings, for instance the cambered and uncambered gothic wings of Ref. 10, and it appears that in a small incidence range on either side of the attachment incidence the flow behaves to some extent as if attached, and the leading-edge vortex regime is not fully established until higher incidence. There is a corresponding effect on lift-curve slope, Fig. 4, particularly at $M = 1 \cdot 4$ where there is a fairly sudden increase of slope near $\alpha = \pm 1\frac{1}{2}°$. The pressure distributions of Fig. 14a for $M = 1 \cdot 4$, $\alpha = 1°$, show that at $y/s_T = 0 \cdot 55$, and further inboard, any suction peaks due to leading-edge separation are of very limited chordwise extent; they do not affect the first pressure-plotting point at $0 \cdot 025$ of the local chord. At $y/s_T = 0 \cdot 8$, however, the peak suction region extends back to $0 \cdot 15$ of the local chord, so that at very small incidences it appears that the effects of separation may be confined to the outer parts of the wing, with little effect on overall forces.

On the present plane wing, at any rate, the reductions in stability are confined to lift coefficients of less than $0 \cdot 02$ and so would not be of operational significance on an aircraft designed to cruise at a lift coefficient of around $0 \cdot 075$ at Mach numbers of 2 or more. Also, an operational aircraft would have its centre of gravity about $0 \cdot 1\bar{c}$ further forward than the axis position used in Fig. 7, because of low-speed stability requirements, and would therefore have a positive stability margin of about $0 \cdot 09\bar{c}$ in the kink region instead of the instability shown in Fig. 7. The small stability changes near the attachment incidence are thus not likely to cause any operational difficulty in themselves. However, it is obviously undesirable for an aircraft to cruise in this region of fairly rapid change of leading-edge flow characteristics near attachment, and this means that, in the design of cambered wings, there should be a sufficient margin between the cruising lift coefficient and the attachment lift coefficient to ensure a properly developed leading-edge flow at cruise.

In Fig. 8, showing the variation of centre of pressure with Mach number at $C_L = 0 \cdot 075$, results are given both allowing for and ignoring the inflection near $C_L = 0$, and the difference is generally less than $0 \cdot 005c_0$. The centre of pressure is at about $0 \cdot 698c_0$ for Mach numbers of $1 \cdot 4$ to $2 \cdot 0$, moving forward slightly to $0 \cdot 691c_0$ by $M = 2 \cdot 8$. The value given by slender-wing theory for attached flow is about $0 \cdot 05c_0$ further forward, at $0 \cdot 64c_0$. As shown in Fig. 8, this is the same as the measured centre-of-pressure position for subsonic speeds.

If the aircraft centre of gravity is chosen so as to give at worst neutral stability for take-off and landing, then the difference between the cruising centre-of-pressure position and the low-speed aerodynamic-centre position at $C_L \sim 0 \cdot 5$ represents the minimum forward shift of the centre of pressure required, from camber or flaps, for trim under cruising conditions*. For the present wing this amounts to a forward shift of $0 \cdot 074c_0$, i.e. a ΔC_m based on c_0 of $+0 \cdot 0055$ for a typical cruising C_L of $0 \cdot 075$. It should be noted, however, that the cambered version of the present wing, which was designed earlier, is intended to give a ΔC_m based on c_0 of only $0 \cdot 0026$, i.e. about half what would now seem to be required assuming no changes in stability due to camber.

4.3. *Drag.*

4.3.1. *Wave drag at zero lift.*—As can be seen in Fig. 9, at the test Reynolds number of 10^7 based on c_0 about two-thirds of the total zero-lift drag is skin friction, and only the remaining one-third is wave drag. A reliable estimate of the friction drag is therefore needed in order to derive the wave drag accurately. In Fig. 9 the mean skin-friction coefficient over a chord-length 'c' has been calculated from equations (5) and (7) of Ref. 7 for a flat plate with fully turbulent boundary layer and zero heat transfer, giving

$$(C_F)_c = 0 \cdot 074 R_c^{-1/5} \left[1 + \sigma^{1/3} \frac{\gamma - 1}{2} M_0^2\right]^{(n-3)/5} \quad (2)$$

$$= 0 \cdot 074 R_c^{-1/5} G(M_0), \text{ say} \quad (3)$$

where

R_c = Reynolds number based on local chord

σ = Prandtl number

assuming $\sigma = 0 \cdot 72$ and $n = 0 \cdot 76$. The overall skin-friction coefficient has been obtained by integrating equation (3) stripwise across the span to give

$$(C_F)_{\text{wing}} = 0 \cdot 074 R_{c_0}^{-1/5} \lambda G(M_0) \quad (4)$$

where

$$\lambda = \frac{1}{p} \int_0^1 \left(\frac{c}{c_0}\right)^{4/5} d\eta$$

$$= 1 \cdot 125 \text{ for the present planform}$$

and

R_{c_0} = Reynolds number based on root chord.

---

* Assuming no effect of camber or flaps on stability.

The friction drag is then given by

$$C_{DF} = \left(\frac{\text{Total wetted area}}{\text{Planform area}}\right) \times (C_F)_{\text{wing}}. \qquad (5)$$

The mean value of C_F is sometimes calculated by using a mean value of R based on $\bar{c}$ or $\bar{\bar{c}}$ in equation (3), instead of integrating the values based on local chord as in equation (4). For the present planform, the use of $\bar{c}$ or $\bar{\bar{c}}$ in equation (3) would give friction drags 2% larger and 2% smaller, respectively, than the strip method used here. The differences are quite small, but the percentage difference in wave drag is of course twice as great. It should also be noted that both equation (3) and equation (4) are derived for flat plates, i.e. the usual assumption is made that the overall friction drag is unaffected by pressure gradients due to thickness. In equation (5), however, the true wetted area is used rather than twice the plan area as for a flat plate. The increase in area is about 4% for the present model, but for designs with more pronounced central bodies the figure would be larger; in two recent project studies it amounted to about 8%. There does not appear to be any justification for disregarding this factor, as is sometimes done; in fact to do so would lead to inconsistencies in the derived wave drags for models with different central bodies.

The zero-lift wave-drag coefficients $(C_{D0})_w$ derived from the balance tests, using these estimates for skin friction and the sting corrections of Section 3.1, are plotted against Mach number in the top half of Fig. 9; $(C_{D0})_w$ varies from $0 \cdot 0033$ at $M = 1 \cdot 4$ to $0 \cdot 0018$ at $M = 1 \cdot 8$. Also shown in Fig. 9 are the values obtained by integrating the pressure-plotting data and applying a correction for sting interference, and it can be seen that the agreement between the balance and pressure-plotting results is remarkably good. This could mean that the various assumptions made in producing Fig. 9 are correct; on the other hand, it could be due simply to a fortuitous cancelling of errors. In addition to the uncertainties in friction drag and sting corrections already noted, the integration of the pressure-plotting data also involves some uncertainty since the absence of pressure tappings at the leading edge necessitated some extrapolation in this region.

The lower half of Fig. 9 shows the zero-lift wave-drag factor K_0, given by

$$K_0 = \left[\frac{\pi \times (\text{wing area}) \times c_0{}^4}{128 \times (\text{volume})^2}\right] (C_{D0})_w \qquad (6)$$

plotted against Mach number. K_0 varies from $1 \cdot 1$ at $M = 1 \cdot 4$ to $0 \cdot 6$ at $M = 2 \cdot 8$, where its value appears to be roughly a minimum. At $M = 2 \cdot 8$ part of the wing (near $0 \cdot 58 \times$ semispan) is approaching sonic leading-edge conditions, $\beta ds/dx$ being $0 \cdot 9$ in this region; the overall value of $\beta s_T/c_0$ is $0 \cdot 655$ at this Mach number.

Comparing the measured values of K_0 with the results from slender-wing theory shown in Fig. 9, it can be seen that the decrease of K_0 with increasing speed is well predicted by slender theory, and that the measured values of K_0 are less (by about $0 \cdot 2$) than the slender-theory values. In these respects the present wing, with Newby area distribution and $p = \frac{1}{2}$ planform, behaves similarly to earlier wings with Newby or Lord V area distributions and delta, gothic and mild gothic planforms. In contrast, preliminary results on some later wings with more 'necked-in' planforms ($p < \frac{1}{2}$), and area distributions having further-aft maxima and larger trailing-edge derivatives, show that for these planforms the achieved values of K_0 are considerably larger than the slender-theory values.

Linear thin-wing-theory drag calculations have not yet been made, but a few pressure distributions have been calculated, as shown in Fig. 12. If the differences between these and the slender-theory distributions are integrated, assuming the same pressures near the leading edge, it is found that at $M = 2$ the 'linear-theory' value of K_0 is $0 \cdot 92$, compared with $0 \cdot 96$ on slender theory. This comparison must be treated with reserve, however, as the proper linear-theory drag may involve differences near the leading edge, compared with slender theory, which have not been taken into account.

One reason for the smaller measured drag compared with theory on the present wing can be seen from the pressure distributions of Fig. 12. These will be further discussed in Section 5.1, but it may be noted at this stage that both linear and slender theories predict rapidly increasing suctions towards the trailing edge, particularly on the inner part of the wing, and these are not realized experimentally. If the pressure differences at the rear, compared with slender theory, are integrated, and allowance made for the pressure field of the sting shroud which is of course included in the experimental pressures, it is found that they account almost exactly for the drag differences shown in Fig. 9. At $M = 2$, for instance, the observed pressure differences at the rear, compared with slender theory, correspond to $\Delta C_D = 0 \cdot 0010$ and the sting correction is $\Delta C_D = 0 \cdot 0004$, leaving $\Delta C_D = 0 \cdot 0006$ as the true discrepancy; this compares with $\Delta C_D = 0 \cdot 0005$ in Fig. 9*. The spanwise distribution of drag is shown in Fig. 10 and it can be seen that most of the drag, and most of the discrepancy between theory and experiment, is concentrated on the inner part of the wing. Further discussion on this subject will be found in Section 5.1.

4.3.2. *Drag due to lift.*—As noted in Section 3.1, the experimental values of the overall lift-dependent drag factor, K, are different for positive and negative incidences because of tunnel flow effects. Results are given in Fig. 11 for both positive and negative incidences; the differences are fairly small beyond $C_L = 0 \cdot 1$. In the lower part of Fig. 11 the mean values of K at $C_L = 0 \cdot 1$ are plotted against Mach number, and it can be seen that K increases from about $1 \cdot 5$ at $M = 1 \cdot 4$, to $2 \cdot 4$ at $M = 2 \cdot 8$. The measured values agree very well with the mean curve derived in Ref. 7 from experimental results on a number of wings with no camber or with transverse camber only.

The lift-dependent drag factor is sometimes expressed in the form

$$K = K_V + 2 \left(\frac{\beta s_T}{c_0}\right)^2 K_W \qquad (7)$$

K_V being the 'vortex-drag factor' and K_W the 'lift-dependent wave-drag factor'. For the present wing, the values which best fit the supersonic results are $K_V = 1 \cdot 35$, $K_W = 1 \cdot 20$; the corresponding values of K are shown as crosses in the lower part of Fig. 11. For Mach numbers of $1 \cdot 5$ to $2 \cdot 8$ this arbitrary choice of K_V and K_W gives excellent agreement with the experimental results, but the choice of $K_V = 1 \cdot 35$ does not agree with the low-speed results giving $K = 1 \cdot 6$ at $M = 0 \cdot 3$.

With the R. T. Jones lower-bound values of $K_V = K_W = 1$, the value of K at $M = 2$ would be $1 \cdot 38$, compared with a measured value of $1 \cdot 80$ at this Mach number. Thus, although the measured value for this planform is no worse than would be expected from the mean curve of Ref. 5 for uncambered wings, there is evidently scope for reduction of K by suitable camber and twist. Values of K_V and K_W of about $1 \cdot 1$ have already been measured on the uncambered gothic

---

* In view of the uncertainties in measuring and integrating the pressures, and in allowing for skin friction and sting interference, this apparently close agreement could be no more than fortuitous. It should not be taken as conclusive proof that the whole of the discrepancy between theoretical and measured wave drag is attributable to the observed pressure differences near the rear, although these obviously play a large part.

wing of Ref. 8 for instance, and if similar results could be achieved on the present planform by the use of camber and twist, the value of K at a Mach number of 2 would be reduced from $1\cdot8$ to about $1\cdot5$.

4.3.3. *Lift/drag ratio.*—Because of the low Reynolds number and the absence of full-scale items such as fins, etc., the lift/drag ratio given directly by model experiments is of little significance except as a rough means of comparison with other model results. For the present wing, the measured values of $(L/D)_{\max}$ are

$$7\cdot45 \text{ at } M = 1\cdot4$$
$$7\cdot35 \text{ at } M = 2\cdot2$$
$$\text{and } 7\cdot05 \text{ at } M = 2\cdot8\,.$$

The full-scale aircraft will achieve higher values than these, the extra drag of fins and miscellaneous items being more than offset by the reduction of friction drag at the higher Reynolds number. For an aircraft cruising at $M = 2\cdot2$ at high altitude a typical drag coefficient for skin friction, fin and miscellaneous items (but excluding engines) would be about $0\cdot00375$. With $K_0 = 0\cdot72$ and $K = 1\cdot92$, and assuming the same volume coefficient ($\tau = 0\cdot0343$) as for the model, the full-scale value of L/D, excluding engine drag, would be $8\cdot3$ at $M = 2\cdot2$.

5. *Pressure-Plotting Results.*

5.1. *Zero-lift Pressure Distributions.*

Pressure distributions at zero lift are given in Fig. 12 for Mach numbers of $1\cdot4$, $2\cdot0$, $2\cdot4$ and $2\cdot8$, uncorrected for sting interference effects. Two sets of results are given, the circles representing tests with transition free and the small pressure-plotting sting shroud, and the crosses tests with transition fixed and the larger balance sting shroud. All results are for $R = 10^7$ based on c_0; tests at half this Reynolds number at $M = 2$ showed no significant differences.

The effects of fixing transition in Fig. 12 are inconsistent; at Mach numbers of $1\cdot4$ and $2\cdot8$ there is hardly any difference between the results (except at the rear, due to the shroud change) but at Mach numbers of $2\cdot0$ and $2\cdot4$ the values of C_p with fixed transition are about $0\cdot01$ more negative than those with free transition. The inconsistency is probably due to errors in measurement of the type discussed in Section 3.2, affecting the complete set of readings at any one incidence. In Fig. 15, where a similar comparison is given for a number of incidences at $M = 2\cdot0$, the effect of fixing transition is to make C_p fairly consistently more negative on both upper and lower surfaces. It is not clear why fixing transition should have such an effect, but it is not of great importance in the present context. It does not affect the general shape of the measured distributions, or their qualitative agreement or disagreement with theory, and it has little effect on either drag or lift since the pressure change seems to be roughly the same over the whole wing surface. Subsequent discussion will be based on the results with free transition and the smaller sting shroud.

Fig. 12 shows that except near the rear of the model, as noted in Section 4.3.1, the agreement of the measured pressures with theory is qualitatively quite good apart from one or two points near the front of the centre section and near $0\cdot4c_0$ at $y/s_T = 0\cdot125$. It is not known whether the uneven pressure distributions in these areas are genuine or not, since examination of the model after test showed local imperfections in the Araldite filling around the orifices in question, which might have caused them to give a consistently high or low reading. In integrating the distributions it has been assumed that the readings are in fact unrepresentative, and smooth curves have been drawn through them.

Fig. 12 includes theoretical results using both slender-wing theory and linear thin-wing theory. At $M = 1 \cdot 4$, the two theories give very similar results and the measurements agree well with either except towards the rear. With increase of speed both theories predict reductions in the favourable pressure gradients, and a general lowering of suctions over the rear and outer parts of the wing (compare $M = 1 \cdot 4$ and $M = 2 \cdot 8$, for instance), and the experimental results follow these general trends fairly closely. The differences between the two theories increase at the higher Mach numbers, however, linear theory predicting higher suctions on the outer sections and lower suctions near the trailing edge of the inner sections compared with slender theory. Because of the experimental scatter and the differences between transition-fixed and transition-free results, it is not possible to say that one theory gives better agreement than the other at the higher Mach numbers.

One of the aims in the design of this model was to see whether a wing with varying cross-section shapes could be designed, using slender-wing theory, to give smooth pressure distributions and small velocity increments due to thickness, and low drag. At the time, the design of such a wing represented a fairly difficult problem; it was all too easy to produce shapes which, while apparently smooth, gave 'lumpy' pressure distributions. Even when a shape was produced, e.g. the present one, which should give acceptable distributions according to slender theory, there remained the doubt whether the theoretical distributions would be achieved in practice. In this context, the results of Fig. 12 indicate a large measure of success for the design procedures of Ref. 1; the model has achieved smooth pressure distributions and small velocity increments everywhere, there is good agreement between theory and experiment except near the trailing edge, and the drag due to thickness is low.

As noted in Section 4.3.1, part of the apparent difference between the theoretical slender-wing pressures and the measured pressures on the rear part of the inner sections is due to sting-shroud interference; on the assumptions used here this accounts for 30% to 40% of the observed pressure difference, depending on Mach number. The differences remaining after applying this correction are quite large, however, corresponding to $\Delta C_D = 0 \cdot 0006$ at $M = 2$ which represents 25% of the zero-lift wave drag at this speed. Various possible explanations can be thought of for the pressure differences; these are discussed below.

First, there is the question of the adequacy of the sting-interference correction, and in the present context we are concerned only with the pressure-field term of Section 3.1; the term due to the masking of rear-facing surfaces affects only the forces measured on the balance. The correction applied here is based on pressure measurements made on a Lord V delta, with and without a rear sting. These were integrated to give a drag correction due to the sting shroud on that wing, and for the present wing this has been scaled according to the $1 \cdot 6$th power[9] of the effective cone angle of the added volume above the wing surface, according to the amount of rear-facing surface behind the Mach wave from the shroud leading edge, and according to the relative shroud diameters and wing areas, giving a drag correction about twice as large as that for wing F. Preliminary results from pressure measurements with and without sting on a similar model tend to confirm the original figures for the Lord V delta. However, both these wings had thickness distributions giving a fairly flat pressure distribution over the rear of the inner sections. The present wing is the first to be tested with thickness distributions giving rapid increases of suction towards the rear. It is not immediately obvious from the theory which particular features of the thickness distributions of the present wing (Figs. 2 and 3) are mainly responsible for these increases of suction. It seems likely, however, that they are associated with the large streamwise slopes and curvatures towards the rear of the inner sections only, and the consequent heavy concentration of sinks in this relatively small region. It is precisely this region which is masked by the addition of the cylindrical sting shroud. In scaling the Lord V delta sting correction some account has been taken of this factor, by introducing the equivalent cone angle of the added volume above the wing surface, but it may be that the allowance is inadequate, and further theoretical and experimental work is desirable. The most useful source of information would of course be pressure-plotting tests with and without sting, as for the two wings already mentioned.

At any rate in principle, a second reason for the observed pressure differences might be boundary-layer thickening towards the rear of the wing. Unpublished work by Prof. J. C. Cooke, however, indicates that the theoretical effect of this would be much less than the observed discrepancy unless boundary-layer separation were present. In this respect, moreover, the present wing would be expected to behave better than other wings which have been pressure-plotted, rather than worse, as measured, because of the strong favourable pressure gradients predicted by theory.

A third possibility is that of interaction between the trailing-edge shock and the boundary layer, reducing the shock strength and the expansion ahead of the shock compared with theoretical predictions. Unfortunately the boundary-layer behaviour on the wing surface cannot be seen in the schlieren pictures of Fig. 25 because of the sting shroud, but if such interaction occurred one would expect to be able to see either a forward movement of the shock ahead of the trailing edge, or a bifurcated shock with a forward limb ahead of the trailing edge. Neither of these features is apparent in Fig. 25.

The final possibility is that the pressure differences are due simply to theoretical deficiencies. The limitations of slender theory are well known, but in the present case the slender-theory results are quite similar to those from linearized thin-wing theory (Fig. 12) and the latter must also be questioned. One feature of linear thin-wing theory in the present context is the thinness assumption by which the boundary conditions are satisfied in the chord plane rather than on the surface. The errors introduced by this assumption on the present wing, with its faired central body and consequent 'lumpy' cross-sections, Fig. 2, would be expected to be greater than those for earlier wings with simple cross-sections. However, although no results are available without this simplifying assumption, it is generally considered that the errors introduced by it should not be as great as the difference of $0 \cdot 1$ in C_p implied by Fig. 12a for instance.

No further possibilities can be suggested, and the choice therefore seems to lie mainly between inadequate sting corrections and inadequate theory—with a general feeling in the latter case that the theory should hardly be wrong to this extent! On the other hand, to attribute the discrepancy entirely to sting effects would involve increasing the assumed sting pressure-field correction by a factor of about $2\frac{1}{2}$. For the balance sting, this would mean almost doubling the total corrections of Section 3.1, so that the sting correction for this type of wing would represent over half the zero-lift wave drag, a most unpleasant state of affairs from the experimental viewpoint. It would seem essential, if further sting-mounted-model tests are contemplated on wings with this kind of thickness distribution, that further pressure-plotting evidence should be obtained with and without the sting and also, perhaps, with and without the central faired body of the present model. In addition, further calculations should be made on wings with 'lumpy' cross-sections, with and without the addition of a cylindrical sting shroud at the rear, using various available methods in order to gain further insight into these rear-end effects and the possible effects of sting interference on them.

Finally, it is perhaps worth noting that over the greater part of the wing, where the velocity increments are small, the agreement between theory and experiment is quite good; it is only where theory predicts fairly large velocities, near the trailing edge, that agreement is poor. This suggests that, apart from the questions of sting interference and the simplified boundary conditions of linear thin-wing theory, the source of the disagreement near the trailing edge might lie in the basic assumption of small perturbations, common to both linear and slender theories, and also perhaps in the approximations, different for the two theories, for the direction of propagation of disturbances. To improve the theories in these respects is of course a matter of considerable difficulty, and as a general principle it is therefore desirable that, as far as possible, design solutions should be sought in which the velocity increments are everywhere small.

5.2. *Lifting Characteristics.*

5.2.1. *Pressure distributions, local load and chord load.*

—Upper-surface and lower-surface chordwise pressure distributions are given in Fig. 14 for incidences of 0 to $8\frac{1}{2}$ degrees and Mach numbers of $1\cdot4$, $2\cdot0$ and $2\cdot8$. These have been integrated to give loading distributions which will be discussed later, but there are several features of the pressure distributions themselves which may be noted.

The chordwise pressure distributions show the usual effect of flow separation from highly swept leading edges, the upper-surface suctions rising to a peak beneath the coiled leading-edge vortex sheet with a rapid increase of pressure further aft along the chord. The effect is much more marked at the lower Mach numbers; with increase of speed the high-suction region beneath the vortex extends rearward and flattens until by $M = 2\cdot8$ it is only just visible. Vapour-screen studies on other wings have shown that this is associated with a marked reduction in the height of the vortex sheet above the wing with increase of speed. The oil-flow pictures of Fig. 23 ($\alpha = 6\cdot4°$) illustrate the accompanying decrease in scrubbing action of the vortex, and the inward movement of the attachment line of the flow over the top of the vortex sheet, as Mach number increases. The observed movement of the attachment line is shown graphically in Fig. 24, and it can be seen that the position of the attachment line corresponds quite closely to the rearward limit of the region of high suction beneath the vortex from Fig. 14, shown as points in the upper half of Fig. 24. Fig. 24 also gives the position of the secondary separation line, which appears to be constant for all Mach numbers, and of the peak-suction line for Mach numbers of $1\cdot4$ and $2\cdot0$; at higher speeds there are no well-defined suction peaks.

Fig. 14 shows that inboard and to the rear of the vortex region the chordwise pressure gradients are generally favourable, even at $8\frac{1}{2}°$ incidence. In this area the effect of incidence seems to be simply to produce a roughly constant pressure increment over the whole chord right back to the trailing edge, so that the pressure gradients are practically the same as those due to thickness alone. This is shown more clearly in Fig. 16, giving the pressure increments due to incidence at $M = 2$ on upper and lower surfaces, for incidences of $2\cdot15°$ and $4\cdot25°$. Also shown for comparison are the results which would be given by slender-wing theory if the flow were attached at the leading edge. (Although in one sense such a comparison might seem rather academic since the flow is not in fact attached, it has some practical interest since the cruising incidence will in general be greater than the attachment incidence, and attached-flow slender theory is sometimes used for the part of the loading beyond the attachment condition.) The biggest difference compared with slender theory is at the trailing edge. Here the theory predicts zero load because of the streamwise tips, but in practice the trailing-edge loads are as great as those further forward on the chord, on both upper and lower surfaces. The distribution to the rear of the vortex region is in fact generally similar to that given by slender theory for a delta wing with no streamwise tip. A full analysis has not been made, but at $M = 2$, taking the mean* of the loadings for $\alpha = 2 \cdot 15°$ and $\alpha = 4 \cdot 25°$, the span of the equivalent delta so far as the loads to the rear of the vortex are concerned would be about $0 \cdot 22c_0$ (compared with $0 \cdot 25c_0$ for the actual wing). The additional load near the trailing edge is of course part of the reason for the further aft centre-of-pressure position, compared with slender theory, noted in Section 4.2. Further discussion on this question will be given later when dealing with the distribution of cross-load.

Another interesting feature of Fig. 14 is that, apart from the high suctions on the upper surface under the vortex core, the rest of the loading is by no means equally distributed between upper and lower surfaces as is usually assumed, but is appreciably greater on the lower surface than on the upper surface. On the centre section at $\alpha = 4 \cdot 25°$, for instance, the ratio of the total chord load on the lower surface to that on the upper surface varies from about $1 \cdot 4$, at $M = 1 \cdot 4$, to as much as $1 \cdot 8$ at $M = 2 \cdot 8$. The ratio decreases further outboard, as shown in Fig. 17, because of the additional vortex lift developed on the upper surface, but at $M = 2 \cdot 8$, where there is little non-linear lift, the lower-surface lift remains greater out to $0 \cdot 7 \times$ semispan. Fig. 17 also gives the results from attached-flow slender theory, assuming equal lift on both surfaces, and it can be seen that the lower-surface lift is always greater than the theoretical value near the centre of the wing, falling below further outboard. The upper-surface lift, on the other hand, is always less than the theoretical value near the centre of the wing.

Spanwise distributions of the total chord load (i.e. both upper and lower surfaces) are given in Fig. 18 for various Mach numbers and incidences. At $M = 2 \cdot 8$, where there is little non-linear lift, the distribution is roughly elliptical, as would be predicted by slender theory, but with a hump near the centre caused by the extra lower-surface lift. As is to be expected at this high speed ($\beta s_T/c_0 = 0 \cdot 65$), the overall lift is of course appreciably less than the slender-theory value, as noted earlier (Fig. 6). At lower Mach numbers, the effects of the non-linear lift developed on the outer sections become apparent, and the spanwise load distributions become rather more rectangular in shape. The number of pressure-plotting stations was insufficient to determine the shape of the distributions on the outer parts of the wing, and the points are therefore left unconnected in Fig. 18.

5.2.2. *Cross-load.*—Figs. 19 and 20 present some typical spanwise distributions of local load at various chordwise positions, and Figs. 21 and 22 give chordwise variations of cross-load obtained by integrating such distributions. The results from attached-flow slender-wing theory are also shown, and the loads are divided by incidence or by total load to facilitate comparison.

Fig. 19 shows the effects of incidence at a Mach number of $2 \cdot 0$. On the inner parts of the wing $\Delta C_p/\alpha$ is about the same for all incidences, as would be expected, and differs from the slender-theory values at the various chordwise positions in the manner discussed in the previous section. Near the leading edge the values of $\Delta C_p/\alpha$ at the lowest incidence ($\alpha = 2 \cdot 15°$) follow in a qualitative manner the $\sqrt{(1-\eta^2)}$ trend of slender theory, but with the theoretically infinite leading-edge suctions replaced by finite suction peaks representing the beginning of the effects of the leading-edge vortex system. As can be seen also in the chordwise pressure distributions of Fig. 14, increase of incidence does not produce simply a linear increase of pressures and local loads, which would leave the height

* The consistent difference between the lower-surface values of $\Delta C_p/\alpha$ for the two incidences is thought to be due to experimental error of the kind discussed in Section 3.2.

and shape of the peak-loading region the same in terms of $\Delta C_p/\alpha$; instead the peak decreases in height and becomes wider. This marked alteration in shape of the peak with increase of incidence at $M = 2$ takes place in such a way as to leave the integrated cross-load virtually unchanged at each chordwise station, as shown in Fig. 21. As noted earlier, there is not much non-linear overall lift at $M = 2$; if there had been there would of course have been greater changes in cross-load/α with incidence.

Fig. 20 shows the effects of Mach number at a constant incidence of $4 \cdot 25°$, and demonstrates the collapse of the high loading peak near the leading edge with increase of Mach number. By $M = 2 \cdot 8$ at this incidence the spanwise distribution of local load is similar in shape to that given by attached-flow slender-wing theory, although the general level of load is of course lower corresponding to the smaller overall lift slope compared with slender-wing theory.

It has been noted previously that at $M = 2$ the overall lift curve displays little non-linear lift in the usual sense of increase of lift slope with incidence, and that the measured lift is in good agreement with that given by linear theory for the equivalent cropped delta. It is perhaps worth remarking that, as discussed above, the actual pressure and load distributions include quite large 'non-linear' contributions in the sense of concentrated loadings under a leading-edge vortex. It happens that these non-linear effects near the leading edge combine with loadings elsewhere on the wing to produce a more or less linear variation of lift with incidence at the higher Mach numbers; the good agreement with linear theory at $M = 2$ could to this extent be regarded as fortuitous.

Distributions of cross-load divided by incidence for various Mach numbers and incidences are given in Fig. 21a, together with the results from attached-flow slender theory. At $M = 1 \cdot 4$ the measured cross-load agrees fairly well with theory over the front two-thirds of the length. Towards the trailing edge, however, as already noted, the loads are very much greater than those given by theory, and this is true at all Mach numbers. Increase of speed leads to a steady reduction in cross-load at all chordwise positions, with little change in general shape. This is shown more clearly in Fig. 21b where the cross-load distributions are made non-dimensional with the total load $\bar{L}$, and it can be seen that at $\alpha = 4 \cdot 25°$ the points for all Mach numbers collapse into a single curve, corresponding to the more or less constant centre-of-pressure position measured in the balance tests (Fig. 8). [There is of course no *a priori* reason why the cross-loads for different Mach numbers should collapse in this manner. The large variation of the leading-edge vortex lift with Mach number might conceivably have produced variations of cross-load distribution and centre of pressure, and the amount of trailing-edge load could also have varied with Mach number. It so happens that on the present wing the variation of the leading-edge vortex lift with Mach number is roughly the same at all chordwise positions (i.e. quasi-conical), and also the trailing-edge load parameter $L(1)/\bar{L}$ does not vary significantly with Mach number, so that the shape of the loading curve is unaltered.] The trailing-edge load parameter $L(1)/\bar{L}$ has the comparatively high value of about $1 \cdot 75$, and compared with attached-flow slender-wing theory there is a shift of load from the front 80% of the length to the rear 20% corresponding to the difference of about $0 \cdot 055c_0$ in centre of pressure measured in the balance tests (Fig. 8).

Mention was made in the previous section of the differences between the measured local loads and those from slender-wing theory, Fig. 16. It appears from a comparison of Fig. 16 and Fig. 21b that the general pattern of the local load discrepancies on the centre-line is similar to that shown by the overall cross-loads, the loads in both cases being less than the theoretical near mid-chord and greater near the trailing-edge. This suggests a possible correlation between the two loadings, as shown in Fig. 22. The lower half of Fig. 22 gives distributions of $-\Delta C_p/\alpha$ at the centre-line for Mach numbers of $1 \cdot 4$, $2 \cdot 0$ and $2 \cdot 8$, and compares them with slender-theory values. (Because of pressure measuring inaccuracies as discussed in Section 3.2 the experimental values used are the mean of those for $\alpha = 2$, 4 and 6 degrees, with transition both fixed and free, for increased accuracy.) In the upper half of Fig. 22 the measured values of cross-load divided by α are scaled up or down in the ratio of the measured to the theoretical values of $-\Delta C_p/\alpha$ at the centre-line at each streamwise position, and it can be seen that when this is done the scaled cross-loads collapse quite closely into the curve given by slender theory. In other words, the departure of the measured cross-load from slender theory at any streamwise position is in direct proportion to the departure of the measured centre-line local load from theory. This link between the measured and theoretical cross-load and the measured and theoretical centre-line load is somewhat remarkable in view of the quite different shapes of the spanwise load distributions for different Mach numbers, arising from differences in leading-edge vortex development (Fig. 20). In the absence of separated-flow effects, slender theory would of course predict that the cross-load should be proportional to the local load at the centre-line. The implication of Fig. 22 is that, at any rate on this wing, the same is true even when a large part of the lift is associated with the leading-edge separation vortex, although there is no obvious reason why variations in leading-edge vortex development should be so closely reflected in differences of local load at the centre-line. It may be that the apparent close correlation on the present wing is to some extent accidental. If it were generally true it would mean that the cross-load distribution and centre of pressure could be accurately predicted, even with separation effects, given an improved method of estimating the centre-line load only.

Finally, mention should be made of the implications of the discrepancies between experiment and slender-wing theory on the problem of camber design for trim at cruising conditions. The $0 \cdot 05c_0$ discrepancy in supersonic centre of pressure, as such, is not important here, because the design requirement for the camber is not to achieve a given centre-of-pressure position in absolute terms, but simply to produce a ΔC_m sufficient to trim the aircraft under cruising conditions at a centre of gravity dictated by low-speed conditions. The requirement is based on the *difference* between low-speed and high-speed conditions rather than on an absolute centre of pressure. Provided the design method gives the required ΔC_m, discrepancies between theoretical and experimental centres of pressure are of no direct consequence. They may be of some significance indirectly, however, since if the plane-wing centre of pressure and load distributions—particularly the latter—differ widely from the slender-theory predictions, there is obviously more reason to doubt whether slender theory will produce the required ΔC_m due to camber. The cambered version of the present wing, for instance, was designed to give a trailing-edge load of $L(1) = 0 \cdot 5\bar{L}$ according to slender theory, the corresponding plane-wing value being zero. In the event, the plane wing has been found to have $L(1) = 1 \cdot 75\bar{L}$ to begin with, and with such a difference on the plane wing the effect of camber on the trailing-edge load could well be quite different from that predicted. When the cambered-wing pressure-plotting results are available it will be interesting to see to what extent the predicted changes in loading due to camber are realized despite the discrepancies on the plane wing.

6. *Conclusions.*

The main points of interest from the overall force results are as follows:

(i) The difference between the supersonic centre-of-pressure position and the low-speed aerodynamic-centre position at $C_L = 0 \cdot 5$ is about $0 \cdot 075c_0$, in good agreement with the figure of $0 \cdot 07c_0$ which has been suggested as a camber design requirement.

(ii) The zero-lift wave drag falls with increase of speed in the manner predicted by slender-wing theory, and the values of K_0 are less (by about $0 \cdot 2$) than the slender-theory values. In these respects the results are similar to earlier results on slender wings with Newby or Lord V area distributions and relatively 'smooth' leading-edge planform shapes. At a Mach number of $2 \cdot 2$ the value of K_0 is $0 \cdot 72$.

(iii) The values of the lift-dependent drag factor, K, are in close agreement with the mean curve of Ref. 5 for wings with no streamwise camber. At $M = 2 \cdot 2$ the value of K at a lift coefficient of $0 \cdot 1$ is $1 \cdot 92$.

(iv) With a typical full-scale drag coefficient of $0 \cdot 00375$ for friction, fin and miscellaneous items, and assuming the same volume coefficient as for the model ($\tau = 0 \cdot 0343$), the estimated maximum full-scale lift/drag ratio at $M = 2 \cdot 2$ is $8 \cdot 3$, excluding engine drag.

The pressure-plotting tests for Mach numbers of $1 \cdot 4$ to $2 \cdot 8$ and incidences up to $6 \cdot 4°$ show that:

(i) One of the main design objectives, to produce smooth pressure distributions, small velocity increments, and low wave drag due to thickness on a varying-section design more representative of a practical aircraft layout, is successfully achieved.

(ii) At zero lift, the measured pressures over the front two-thirds of the model agree quite well with the predictions of either slender-wing or linear thin-wing theory, but near the trailing edge the high suctions predicted by both theories are not present, the differences being sufficient to account for the lower measured drag compared with theory. The integrated pressure drag agrees well with the wave drag deduced from the balance tests.

(iii) The difference between theory and experiment near the trailing edge is thought to be due either to inadequate sting correction or to inadequate theory. If it is due to inadequate sting correction, it implies that on this wing the sting correction should be roughly doubled; it would then amount to over half the zero-lift wave drag. Further experimental and theoretical work is evidently desirable.

(iv) At incidence, the chordwise pressure gradients are everywhere favourable apart, of course, from the pressure changes through the leading-edge vortex system.

(v) Between the reattachment line and the trailing edge the local load due to incidence at any spanwise station is more or less constant over the whole chord right back to the trailing edge. This is what would be expected on a delta wing with no streamwise tips; the decrease of load to zero at the trailing edge, predicted by slender theory for streamwise tips, does not occur, and the trailing-edge cross-load parameter $L(1)/\bar{L}$ has the relatively high value of about $1 \cdot 75$.

(vi) Despite large variations in shape of the local load distributions in the leading-edge vortex region with Mach number and incidence, the non-dimensional cross-load distribution $L(x)/\bar{L}$ hardly varies with Mach number or incidence; changes in the vortex region combine with changes further inboard to leave $L(x)/\bar{L}$ unaltered, giving a more or less constant centre-of-pressure position for Mach numbers of $1 \cdot 4$ to $2 \cdot 8$ and incidences of between 1° and 6°. Because of the large trailing-edge load the centre of pressure is about $0 \cdot 05 c_0$ behind the slender-theory value.

(vii) It appears that at any chordwise position, the departure of the cross-load from the slender-theory value is in almost exact proportion to the departure of the local load at the centre-line from the theoretical value. This apparent link between cross-load and centre-line load is somewhat remarkable in view of the large variation of the leading-edge vortex contribution with Mach number.

LIST OF SYMBOLS

A	=	$4s_T^2/P$, aspect ratio
c		Chord
c_0		Centre-line chord
$\bar{c}$	=	$P/2s_T$, geometric mean chord
$\bar{\bar{c}}$	=	$\int c^2 dy/P$, aerodynamic mean chord
C_D		Drag coefficient based on P
C_{D0}		Drag coefficient at zero lift
C_{DF}		Overall skin-friction drag coefficient based on P
C_F		Skin-friction coefficient per unit wetted area
$(C_F)_c$		Mean value of C_F over local chord length c
$(C_F)_{\text{wing}}$		Mean value of C_F over wing surface
C_p	=	$(p-p_0)/\frac{1}{2}\rho V_0^2$, local pressure coefficient
ΔC_p	=	$(C_p)_{\text{u.s.}} - (C_p)_{\text{l.s.}}$, local load coefficient $\times(-1)$
$(\Delta C_p)_{\text{u.s.}}$	=	$(C_p)_{\text{u.s.}}(\alpha) - (C_p)_{\text{u.s.}}(\alpha = 0)$, contribution of upper surface to ΔC_p
$G(M_0)$	=	$\left[1 + \sigma^{1/3}\frac{\gamma-1}{2}M_0^2\right]^{(n-3)/5}$
K	=	$\pi A(C_D - C_{D0})/C_L^2$, overall lift-dependent drag factor
K_V		Vortex drag factor, Section 4.3.2
K_W		Lift-dependent wave-drag factor, Section 4.3.2
$L(x)$	=	$\int_{-s(x)}^{s(x)} - \Delta C_p(x, y)dy$, cross-load
$L(1, y)$	=	$\int_{\text{L.E.}}^{\text{T.E.}} - \Delta C_p(x, y)dx$, total chord load
$\bar{L}$	=	$\int_0^1 L(x)dx$, total load
M, M_0		Free-stream Mach number
n		Constant, equation (2), assumed $= 0{\cdot}76$
p	=	$P/2s_T c_0$
P		Total planform area
R		Reynolds number
R_c		Reynolds number based on local chord
R_{c_0}		Reynolds number based on centre-line chord
$s(x)$		Local semispan

s_T		Semispan at trailing edge
x		Streamwise distance from apex $\div c_0$
y		Spanwise distance from centre-line
β	=	$\sqrt{(M^2-1)}$
γ	=	$1 \cdot 4$, ratio of specific heats
λ	=	$\frac{1}{p}\int_0^1 \left(\frac{c}{c_0}\right)^{4/5} d\eta$
σ		Prandtl number, assumed $= 0 \cdot 72$
τ	=	$(\text{Volume})/P^{3/2}$
η	=	y/s_T

REFERENCES

No.	*Author(s)*	*Title, etc.*
1	R. V. Clark	Aerodynamic design of wind tunnel models of ogee planform. Handley Page Report Aero. 343. November, 1959.
2	P. C. H. White and J. B. Edwards	Design studies of supersonic civil transports. Handley Page Report R.H.71. January, 1957.
3	J. Weber	Design of warped slender wings with the attachment line along the leading edge. R.A.E. Tech. Note Aero. 2530. A.R.C. 20,051. September, 1957.
4	A. L. Courtney	Some calculations of shape, pressure distribution and drag due to lift for a 'mild ogee' wing with prescribed centre of pressure position. R.A.E. Tech. Note Aero. 2655. A.R.C. 21,954. October, 1959.
5	A. L. Courtney	A collection of data on the lift-dependent drag of uncambered slender wings at supersonic speeds. A.R.C. 22,371. July, 1960.
6	A. Stanbrook	The lift-curve slope and aerodynamic centre position of wings at subsonic and supersonic speeds. R.A.E. Tech. Note Aero. 2328. A.R.C. 17,615. November, 1954.
7	R. J. Monaghan	The choice and presentation of formulae for turbulent skin friction in compressible flow. R.A.E. Tech. Note Aero. 2246. May, 1953.
8	L. C. Squire	An experimental investigation at supersonic speeds of the characteristics of two gothic wings, one plane and one cambered. A.R.C. R. & M. 3211. May, 1959.
9	Z. Kopal	*Tables of supersonic flow around cones.* Massachusetts Institute of Technology. 1947.

TABLE 1

Values of $10^3 C_p$: Transition Free, Small Sting Shroud, $R = 2 \times 10^6/ft$

(*a*) $M = 1 \cdot 4$

α(degrees)

$10^3 y/s_T$	$10^3 x/c_0$	−12·86	−8·54	−6·41	−4·27	−3·19	−2·12	−1·06	0	0	1·06	2·12	3·19	4·27	6·41	8·54	12·86
0	109	183	170	136	115	108	99	89	82	80	74	63	58	56	+50	+36	+12
	200	187	121	90	67	60	51	39	31	29	24	15	10	+5	−7	−26	−59
	300	199	131	101	74	63	51	39	29	29	20	+8	+2	−4	−14	−34	−71
	400	192	119	89	58	48	36	24	+12	+12	+3	−9	−16	−23	−36	−55	−99
	500	184	109	77	46	34	20	+7	−5	−5	−14	−26	−34	−43	−55	−76	−124
	600	176	101	69	37	23	+11	−5	−19	−17	−27	−41	−51	−58	−74	−94	−147
	700	151	81	47	15	+1	−11	−26	−38	−38	−49	−62	−72	−79	−97	−117	−169
	750	117	73	40	8	−4	−18	−32	−47	−49	−56	−71	−81	−90	−105	−128	−176
065	148	172	131	113	95	86	77	71	62	60	53	41	34	26	9	9	−216
	193	179	128	106	83	71	60	52	41	36	31	19	10	3	12	31	+49
	238	188	130	103	76	65	55	45	33	31	21	9	2	7	22	40	70
	283	193	126	99	71	60	48	38	26	24	17	7	2	10	26	43	78
125	204	166	135	120	103	98	88	79	66	62	54	36	21	+9	−117	−189	−278
	224	182	136	116	95	86	74	64	52	50	40	24	+10	0	−12	−187	−377
	244	188	135	111	88	77	65	50	36	33	24	9	−3	−14	−29	−38	−393
	265	201	140	113	86	72	62	48	34	33	+24	+10	−2	−12	−27	−33	−302
	306	175	107	80	48	38	27	17	3	2	−7	+21	−31	−40	−57	−71	−146
	428	209	132	100	68	58	46	30	+15	17	+5	−7	−18	−26	−43	−64	−99
	469	195	116	84	52	40	26	+12	0	+2	−10	−24	−32	−41	−60	−81	−122
	510	177	104	70	39	27	13	−2	−14	−12	−24	−36	−46	−55	−72	−93	−134
	592	172	97	63	28	17	+3	−10	−24	−24	−34	−48	−58	−67	−86	−106	−158
	673	157	87	53	21	+7	−7	−21	−34	−34	−45	−58	−68	−77	−96	−117	−167
	755	131	69	37	+5	−11	−24	−38	−52	−52	−62	−78	−88	−95	−114	−133	−185
	796	121	60	27	−5	−19	−33	−46	−60	−58	−71	−84	−94	−101	−120	−141	−191
	837	155	73	39	+6	−7	−21	−33	−47	−49	−57	−71	−81	−93	−112	−136	−190
	878	150	73	41	+7	−5	−17	−31	−41	−43	−53	−65	−77	−88	−107	−129	−183
	918	131	56	25	−5	−17	−31	−43	−55	−57	−66	−79	−87	−94	−115	−139	−191
	959	129	58	27	−4	−16	−28	−40	−50	−54	−60	−72	−82	−91	−112	−136	−195

330	397	213	164	139	109	97	83	62	38	36	17	−39	−130	−161	−227	−283	−354
	412	222	159	127	89	81	65	45	22	19	+5	−15	−109	−192	−247	−295	−382
	428	218	150	118	86	72	57	38	+12	+9	−2	−22	−36	−173	−287	−316	−398
	443	222	147	111	79	65	48	29	−2	0	−9	−27	−27	−79	−299	−371	−396
	473	213	135	99	62	48	33	14	−5	0	−21	−40	−48	−41	−230	−378	−417
	504	208	127	92	55	41	25	+8	−11	−9	−24	−43	−53	−57	−52	−318	−499
	535	199	119	82	46	32	15	0	−16	−16	−31	−48	−60	−69	−62	−132	−527
	566	196	112	77	39	27	10	−5	−21	−21		−52	−63	−72	−76	−84	−457
	597	194	111	75	38	22	+5	−11	−26	−21	−40	−55	−67	−74	−86	−91	−367
	628	184	100	65	29	15	0	−17	−31	−26	−45	−60	−72	−79	−95	−101	−280
	690	173	92	56	20	+8	−7	−23	−38	−35	−50	−66	−74	−84	−102	−119	−205
	752	155	75	41	+6	−6	−19	−35	−49	−45	−61	−74	−82	−91	−109	−129	−183
	814	141	63	29	−4	−16	−30	−45	−57	−54	−71	−83	−93	−101	−121	−145	−195
	876	153	68	32	−4	−16	−30	−43	−57	−57	−69	−83	−93	−103	−122	−148	−191
	907	148	71	37	+5	−7	−21	−36	−50	−52	−60	−74	−86	−96	−115	−139	−191
	938	136	63	30	−2	−12	−26	−40	−50	−54	−62	−74	−84	−93	−112	−133	−186
	969	127	56	23	−7	−20	−30	−42	−54	−59	−64	−76	−86	−93	−114	−136	−192
550	560	228	191	169	127	113	94	67	31	31	+10	−148	−173	−206	−261	−301	−381
	571	226	172	145	110	92	72	46	15	15	−9	−150	−185	−215	−272	−315	−390
	582	235	170	138	105	86	55	31	+3	+3	−14	−74	−204	−223	−278	−326	−395
	593	227	155	123	84	67	43	19	−7	−7	−29	−50	−222	−242	−289	−339	−410
	616	218	143	106	67	48	27	+5	−19	−21	−40	−53	−185	−268	−321	−347	−447
	639	208	130	92	53	36	17	−5	−28	−26	−46	−64	−67	−261	−352	−374	−455
	661	198	119	82	45	26	7	−11	−35	−31	−53	−74	−58	−179	−364	−414	−447
	684	199	117	81	44	27	8	−11	−33	−30	−49	−69	−67	−60	−351	−435	−452
	707	192	109	73	34	19	+1	−18	−38	−35	−52	−71	−74	−48	−391	−430	−464
	729	186	104	68	31	+15	−2	−21	−41	−41	−55	−74	−81	−69	−191	−404	−473
	774	171	87	51	15	0	−15	−33	−45	−41	−64	−81	−91	−91	−77	−306	−521
	819	160	78	42	8	−6	−21	−38	−52	−50	−69	−85	−93	−98	−96	−174	−525
	864	146	69	37	+3	−11	−24	−40	−52	−54	−66	−83	−91	−100	−103	−127	−463
	910	152	66	32	−2	−14	−29	−45	−57	−60	−69	−84	−94	−103	−110	−122	−384
	932	147	67	31	−3	−19	−33	−46	−60	−62	−72	−86	−97	−105	−119	−125	−355
	955	138	65	33	2	−12	−24	−38	−51	−57	−63	−77	−87	−96	−110	−122	−314
	977	126	59	30	1	−11	−23	−35	−47	−54	−59	−71	−79	−89	−103	−121	−292
800	761	184	126	99	66	48	29	+5	−29	−26	−88	−197	−224	−254	−302	−343	−414
	774	194	132	100	63	44	23	−1	−30	−28	−57	−212	−228	−254	−310	−349	−412
	788	186	118	86	48	29	12	−12	−38	−34	−63	−223	−248	−262	−312	−362	−422
	801	187	117	85	48	31	12	−9	−35	−35	−57	−206	−262	−271	−311	−364	−429
	814	179	107	75	38	22	+3	−15	−38	−38	−62	−163	−272	−293	−317	−360	−444
	841	174	99	65	28	12	−3	−24	−45	−43	−63	−69	−270	−322	−342	−361	−473
	867	156	90	56	20	+6	−11	−28	−47	−49	−64	−62	−217	−328	−380	−380	−471
	894	143	75	44	+12	−4	−19	−35	−52	−54	−67	−74	−123	−309	−395	−397	−459
	947	118	48	19	−9	−19	−29	−40	−52	−57	−64	−76	−67	−144	−388	−431	−433
	973	99	39	15	−5	−14	−22	−33	−46	−48	−57	−67	−60	−84	−352	−441	−408

TABLE 1—*continued*

(*b*) $M = 1 \cdot 8$

α(degrees)

$10^3y/s_T$	$10^3x/c_0$	−12·74	−8·49	−6·36	−4·23	−3·17	−2·11	−1·06	0	0	1·06	2·11	3·17	4·23	6·36	8·49	12·74
0	100	178	163	133	108	98	88	80	71	72	68	63	55	50	+ 40	+ 27	+ 12
	200	177	117	85	63	53	40	28	26	28	18	13	8	+ 3	− 10	− 26	− 45
	300	182	119	85	58	48	40	33	25	27	16	+ 13	+ 5	− 2	− 17	− 31	− 57
	400	174	108	76	53	41	26	18	+ 8	9	+ 3	− 2	− 11	− 19	− 36	− 53	− 81
	500	174	107	74	47	33	21	+10	0	+ 1	− 5	− 12	− 20	− 29	− 46	− 61	− 94
	600	160	95	61	33	21	+ 7	− 3	−13	−13	−19	− 25	− 35	− 43	− 60	− 79	−112
	700	146	81	48	19	6	− 6	−16	−28	−26	−34	− 39	− 48	− 56	− 75	− 95	−128
	750	135	79	43	16	2	−11	−21	−33	−33	−39	− 45	− 53	− 63	− 82	−102	−131
065	148	174	129	102	84	74	64	59	47	49	43	37	27	17	− 2	− 17	−191
	193	179	123	92	69	59	49	40	29	30	25	18	10	+ 2	− 15	− 32	− 38
	238	179	119	87	62	52	42	34	23	25	18	13	5	− 3	− 20	− 35	− 50
	283	176	116	86	61	49	39	29	22	22	14	9	0	− 8	− 25	− 38	− 63
125	204	176	133	111	94	84	74	66	52	56	44	34	19	+ 7	−109	−161	−216
	224	181	133	106	82	71	60	52	42	45	32	23	+ 10	− 2	− 29	−170	−253
	244	179	128	99	74	64	52	40	29	30	20	12	0	− 12	− 25	− 96	−268
	265	188	131	97	72	60	50	39	27	29	18	+ 10	0	− 10	− 25	− 22	−261
	306	162	104	80	55	40	28	16	8	10	1	− 7	− 17	− 29	− 42	− 54	−174
	428	193	123	91	63	51	36	24	+14	14	+ 6	− 3	− 13	− 21	− 38	− 55	− 81
	469	181	111	76	49	36	24	12	0	+ 2	− 5	− 13	− 23	− 32	− 49	− 67	− 97
	510	169	100	66	38	26	13	+ 3	− 9	− 7	−16	− 22	− 31	− 41	− 58	− 76	−109
	592	159	92	59	30	17	+ 5	− 7	−17	−17	−25	− 32	− 42	− 50	− 69	− 88	−119
	673	153	89	52	25	+12	− 2	−13	−23	−23	−32	− 39	− 47	− 57	− 76	− 94	−126
	755	135	73	36	9	− 4	−17	−28	−39	−38	−47	− 53	− 63	− 71	− 90	−108	−138
	796	127	65	30	3	−10	−23	−34	−45	−44	−50	− 59	− 67	− 77	− 94	−115	−144
	837	132	61	28	1	−12	−26	−36	−46	−43	−52	− 61	− 70	− 80	− 98	−117	−148
	878	137	68	33	+ 6	− 5	−19	−29	−39	−36	−45	− 54	− 64	− 73	− 91	−113	−146
	918	127	58	25	− 2	−15	−27	−37	−47	−44	−52	− 59	− 69	− 79	− 95	−117	−151
	959	127	62	28	+ 1	−12	−24	−34	−44	−42	−50	− 57	− 66	− 76	− 95	−113	−148

330	397	212	160	135	109	94	78	59	39	42	19	−27	−102	−131	−180	−217	−261
	412	215	153	121	91	74	59	40	22	25	+7	−12	−79	−143	−189	−226	−271
	428	212	148	113	83	68	51	32	14	15	0	−15	−42	−127	−204	−237	−283
	443	211	143	112	77	59	44	27	+5	7	−3	−18	−27	−84	−212	−258	−283
	473	201	129	96	62	47	30	15	0	+2	−12	−25	−35	−37	−206	−273	−295
	504	194	122	85	53	38	23	+8	−7	−6	−19	−32	−44	−48	−137	−275	−324
	535	187	114	79	45	30	15	0	−15	−14	−25	−39	−49	−56	−41	−238	−343
	566	181	107	72	40	25	10	−4	−17	−15	−25	−37	−49	−57	−54	−115	−343
	597	177	104	68	37	21	6	−7	−19	−19	−27	−37	−49	−59	−64	−69	−335
	628	172	99	63	32	16	+1	−10	−24	−22	−32	−42	−52	−62	−73	−78	−297
	690	162	88	55	23	+9	−4	−17	−29	−27	−37	−46	−58	−66	−81	−92	−216
	752	145	75	41	13	−1	−14	−26	−36	−34	−42	−53	−61	−71	−85	−102	−161
	814	137	66	33	+3	−11	−23	−34	−44	−41	−51	−61	−71	−81	−97	−117	−160
	876	130	58	24	−4	−17	−31	−41	−53	−49	−59	−66	−76	−86	−103	−122	−153
	907	132	60	23	−4	−19	−31	−42	−54	−51	−59	−67	−78	−86	−105	−125	−156
	938	135	63	28	−1	−14	−28	−38	−49	−46	−54	−63	−73	−83	−100	−119	−150
	969	131	59	26	−3	−16	−28	−38	−48	−45	−54	−63	−72	−82	−97	−119	−150
550	560	241	189	152	124	107	87	63	32	33	+18	−114	−143	−165	−208	−238	−275
	571	230	172	135	105	86	64	43	16	19	−3	−85	−151	−169	−212	−244	−280
	582	231	166	127	90	72	50	30	+6	8	−10	−46	−147	−177	−214	−246	−280
	593	218	152	115	80	62	43	21	0	+1	−19	−41	−141	−185	−219	−251	−283
	616	209	139	100	63	47	28	8	−14	−12	−29	−44	−108	−187	−229	−256	−298
	639	201	128	89	57	37	20	+3	−17	−15	−32	−47	−67	−171	−241	−266	−310
	661	191	117	79	43	27	10	−7	−24	−22	−37	−52	−57	−138	−250	−285	−312
	684	190	116	78	44	26	9	−6	−23	−19	−36	−50	−55	−87	−250	−294	−317
	707	182	108	70	36	19	+4	−12	−27	−24	−41	−54	−61	−58	−250	−302	−325
	729	174	102	63	32	15	0	−17	−31	−25	−42	−56	−64	−57	−241	−305	−323
	774	164	91	54	20	5	−10	−23	−37	−34	−47	−59	−69	−71	−135	−300	−333
	819	155	83	48	16	+1	−12	−26	−39	−38	−51	−61	−71	−76	−54	−252	−342
	864	147	76	41	13	−2	−16	−29	−41	−39	−51	−59	−71	−78	−80	−137	−334
	910	137	67	32	+3	−10	−24	−36	−47	−46	−55	−64	−74	−83	−88	−106	−318
	932	131	60	25	−3	−17	−29	−42	−52	−49	−60	−67	−77	−86	−91	−104	−308
	955	133	61	24	−5	−18	−30	−42	−52	−48	−60	−68	−77	−85	−91	−101	−298
	977	133	63	26	−2	−16	−29	−41	−51	−49	−57	−66	−76	−85	−95	−98	−280
800	761	197	138	104	73	54	34	12	−16	−13	−51	−157	−174	−195	−232	−258	−291
	774	195	134	99	67	49	29	+9	−20	−16	−43	−154	−179	−196	−230	−259	−287
	788	186	123	88	52	37	19	−1	−23	−21	−48	−142	−191	−203	−236	−266	−293
	801	189	122	87	52	35	16	−2	−24	−22	−44	−114	−194	−209	−236	−268	−292
	814	179	111	74	40	24	7	−11	−32	−30	−48	−88	−194	−221	−244	−272	−297
	841	173	104	68	34	17	+2	−15	−32	−30	−48	−53	−185	−230	−252	−269	−308
	867	162	95	58	26	11	−6	−21	−36	−34	−49	−54	−152	−231	−269	−277	−320
	894	149	82	48	16	+1	−14	−27	−41	−39	−52	−59	−91	−219	−285	−293	−327
	947	122	60	29	3	−10	−23	−34	−45	−42	−53	−60	−55	−145	−293	−324	−330
	973	112	52	24	3	−8	−18	−28	−37	−37	−45	−54	−55	−57	−288	−324	−323

TABLE 1—*continued*

(*c*) $M = 2{\cdot}0$

α(degrees)

$10^3y/s_T$	$10^3x/c_0$	−12·68	−8·45	−6·33	−4·22	−3·16	−2·10	−1·05	0	0	1·05	2·10	3·16	4·22	6·33	8·45	12·68
0	100	152	158	142	112	102	88	78	75	73	68	63	57	53	+ 38	+ 31	+ 14
	200	176	118	94	67	59	40	31	23	19	14	9	8	+ 1	− 9	− 18	− 40
	300	178	113	87	59	48	35	28	21	21	+13	+ 6	+ 2	− 1	− 16	− 23	− 50
	400	165	103	80	51	41	24	17	8	8	0.	− 7	− 9	− 19	− 29	− 39	− 68
	500	162	101	74	45	35	18	+ 9	+ 1	+ 1	− 8	− 15	− 20	− 28	− 40	− 50	− 81
	600	150	91	65	34	24	+ 4	− 5	−12	−22	−22	− 27	− 32	− 42	− 54	− 65	− 95
	700	145	87	62	31	21	0	− 8	−15	−17	−25	− 32	− 37	− 46	− 57	− 68	−100
	750	124	85	60	29	17	− 5	−13	−20	−27	−34	− 40	− 42	− 52	− 64	− 73	−102
065	148	173	129	111	85	78	63	56	49	48	41	36	27	15	0	9	142
	193	177	124	102	75	65	48	39	34	31	22	19	10	2	14	24	48
	238	177	116	94	65	55	39	32	24	24	15	9	3	7	19	27	46
	283	173	113	88	59	50	35	25	18	18	8	3	2	11	23	31	55
125	204	178	135	120	96	90	73	64	56	54	42	35	21	+ 8	− 84	−117	−175
	224	184	133	114	87	77	60	53	46	44	29	22	+ 10	− 2	− 27	−102	−193
	244	180	129	105	77	67	48	39	31	29	17	12	0	− 14	− 27	− 75	−198
	265	187	128	104	73	63	46	37	29	27	+15	+ 9	− 2	− 14	− 27	− 32	−195
	306	161	106	86	57	45	28	18	13	9	− 1	− 4	− 15	− 27	− 40	− 44	−172
	428	181	116	90	60	48	31	21	14	14	+ 2	− 3	− 13	− 22	− 35	− 46	− 69
	469	166	105	78	47	39	20	11	+ 4	+ 4	− 8	− 13	− 21	− 30	− 43	− 54	− 86
	510	159	100	74	42	32	15	+ 5	− 2	− 2	−12	− 17	− 26	− 36	− 50	− 60	− 92
	592	153	92	66	36	24	+ 5	− 3	−10	−10	−22	− 27	− 34	− 44	− 58	− 68	− 99
	673	145	87	61	29	19	0	− 8	−17	−19	−29	− 36	− 41	− 53	− 65	− 73	−106
	755	129	78	52	20	8	−12	−21	−28	−33	−41	− 46	− 51	− 63	− 75	− 84	−113
	796	124	73	48	17	+ 5	−15	−25	−31	−36	−42	− 46	− 55	− 65	− 78	− 85	−114
	837	127	64	39	8	− 2	−19	−29	−34	−38	−46	− 51	− 58	− 69	− 84	− 94	−125
	878	135	72	47	16	+ 6	−10	−21	−28	−32	−38	− 45	− 50	− 61	− 76	− 88	−120
	918	128	67	43	11	2	−16	−25	−30	−37	−42	− 47	− 57	− 66	− 79	− 90	−122
	959	127	67	42	11	2	−16	−25	−32	−35	−43	− 49	− 56	− 66	− 79	− 90	−122

330	397	207	158	135	108	97	76	59	44	44	18	−14	−88	−124	−161	−187	−221
	412	206	148	122	90	78	56	42	29	27	+5	−10	−55	−123	−167	−191	−227
	428	205	144	117	83	71	50	33	20	21	−1	−13	−31	−101	−173	−195	−231
	443	204	138	109	73	63	43	29	10	12	−7	−19	−27	−70	−174	−203	−236
	473	192	126	97	63	51	31	15	+7	+9	−12	−24	−34	−43	−171	−213	−242
	504	185	117	88	52	41	22	8	0	0	−19	−29	−40	−46	−140	−207	−246
	535	179	111	81	45	35	14	+2	−6	−6	−25	−33	−44	−52	−66	−185	−271
	566	174	106	77	43	31	11	−1	−10	−8	−25	−33	−44	−52	−45	−139	−264
	597	169	99	69	38	26	6	−6	−13	−15	−26	−37	−47	−56	−59	−68	−271
	628	162	93	64	31	19	+1	−9	−16	−18	−32	−40	−50	−59	−68	−64	−254
	690	154	86	59	27	15	−4	−14	−21	−22	−34	−41	−51	−60	−74	−75	−208
	752	141	76	49	18	8	−9	−19	−24	−28	−38	−44	−53	−62	−74	−80	−156
	814	134	69	42	13	+1	−17	−26	−31	−36	−44	−50	−60	−70	−84	−92	−140
	876	127	64	37	6	−4	−22	−31	−38	−43	−51	−56	−65	−74	−87	−96	−128
	907	127	64	36	6	−4	−23	−33	−40	−44	−50	−57	−64	−74	−88	−97	−131
	938	131	66	40	8	−2	−21	−31	−36	−41	−50	−55	−63	−74	−86	−96	−126
	969	128	63	38	7	−3	−22	−30	−35	−40	−47	−54	−63	−73	−87	−97	+27
550	560	229	179	155	123	110	84	64	38	38	1	−76	−126	−151	−178	−192	−225
	571	226	170	143	108	92	67	46	26	26	+2	−49	−126	−153	−180	−220	−226
	582	227	164	135	93	77	52	33	14	14	−6	−26	−108	−158	−182	−196	−228
	593	215	150	120	82	67	43	26	+8	+8	−16	−30	−103	−161	−185	−201	−231
	616	203	137	104	65	52	30	11	−6	−6	−26	−37	−83	−158	−192	−204	−238
	639	196	128	99	60	46	24	+9	−8	−7	−27	−36	−56	−140	−193	−210	−242
	661	183	116	86	50	35	13	−1	−15	−13	−33	−42	−52	−119	−194	−214	−245
	684	186	114	84	48	34	11	−3	−15	−15	−34	−42	−52	−90	−191	−216	−247
	707	176	107	78	41	27	5	−9	−19	−21	−38	−46	−57	−65	−191	−220	−253
	729	171	103	72	36	25	+2	−11	−23	−23	−38	−47	−57	−57	−187	−219	−257
	774	162	92	63	29	15	−5	−17	−24	−29	−41	−49	−60	−61	−164	−212	−259
	819	154	86	59	25	12	−9	−19	−29	−31	−44	−50	−60	−67	−57	−173	−261
	864	149	81	54	22	10	−9	−19	−29	−31	−43	−50	−58	−67	−60	−138	−253
	910	138	74	47	14	+2	−16	−26	−35	−38	−49	−54	−62	−73	−73	−86	−242
	932	131	70	43	10	0	−19	−29	−36	−41	−49	−54	−63	−72	−73	−80	−234
	955	130	69	44	10	−1	−19	−30	−36	−40	−48	−53	−64	−72	−76	−76	−235
	977	129	66	42	10	−2	−21	−29	−38	−39	−50	−56	−62	−72	−77	−77	−222
800	761	200	144	115	79	64	37	16	−6	−8	−47	−116	−156	−175	−197	−209	−238
	774	197	135	106	73	56	30	13	−9	−11	−40	−104	−156	−176	−197	−209	−236
	788	188	127	98	62	49	23	6	−14	−14	−42	−94	−159	−182	−200	−212	−240
	801	189	127	98	60	45	19	4	−15	−16	−38	−76	−153	−185	−202	−214	−238
	814	173	111	83	44	30	6	+3	−24	−28	−48	−67	−149	−196	−212	−222	−247
	841	175	110	81	45	30	8	−6	−19	−21	−40	−45	−130	−190	−211	−219	−247
	867	163	102	73	37	24	+1	−12	−24	−26	−43	−50	−109	−188	−217	−224	−253
	894	155	93	64	30	16	−6	−18	−28	−37	−45	−52	−76	−187	−221	−231	−254
	947	129	71	46	15	5	−14	−25	−32	−36	−48	−53	−51	−145	−222	−239	−258
	973	117	65	41	14	3	−14	−22	−29	−31	−42	−48	−48	−85	−208	−232	−253

TABLE 1—*continued*

(*d*) $M = 2 \cdot 4$

α(degrees)

$10^3 y/s_T$	$10^3 x/c_0$	−12·56	−8·37	−6·28	−4·18	−3·14	−2·09	−1·05	0	0	1·05	2·09	3·14	4·18	6·28	8·37	12·56
0	100	159	153	130	107	89	81	72	67	65	58	51	45	42	+35	+21	+6
	200	165	113	93	72	53	42	30	26	23	19	10	8	+3	−3	−19	−33
	300	171	109	88	64	44	39	31	24	19	15	+6	+3	−4	−10	−28	−42
	400	157	99	78	60	38	27	20	14	+9	+4	−5	−9	−18	−23	−39	−55
	500	149	91	70	46	28	17	+10	+5	−1	−6	−15	−19	−28	−33	−51	−67
	600	132	81	62	38	18	11	0	−5	−9	−16	−27	−29	−36	−43	−59	−73
	700	120	79	59	37	17	8	−3	−8	−15	−22	−31	−36	−44	−49	−65	−79
	750	89	73	57	39	15	3	−4	−10	−15	−22	−33	−35	−42	−47	−65	−76
065	148	165	125	107	89	72	65	56	50	47	38	29	23	16	+5	−14	−82
	193	163	119	100	80	60	52	41	38	34	27	16	11	+4	−5	−25	−66
	238	163	112	92	71	51	40	36	29	23	18	7	4	−4	−13	−30	−38
	283	164	108	86	64	48	39	30	24	21	12	3	1	−10	−17	−35	−46
125	204	171	131	117	99	84	73	66	60	55	46	31	26	17	−51	−99	−124
	224	184	130	110	91	72	65	56	48	45	34	20	13	+2	−14	−93	−131
	244	175	125	105	82	63	54	45	38	34	23	11	5	−7	−18	−73	−122
	265	179	125	103	80	62	54	41	34	29	22	+9	+4	−9	−20	−52	−118
	306	158	107	86	64	46	39	28	21	17	6	−3	−8	−17	−29	−42	−121
	428	176	109	86	59	41	33	21	14	12	+1	−8	−13	−22	−31	−45	−67
	469	156	97	73	50	30	24	12	4	+3	−8	−17	−22	−28	−39	−55	−72
	510	148	92	71	47	27	18	+7	+2	−2	−11	−21	−25	−32	−41	−57	−73
	592	136	83	62	38	20	11	0	−5	−9	−18	−29	−32	−39	−46	−63	−79
	673	119	78	56	34	13	+2	−7	−13	−18	−25	−36	−39	−46	−54	−70	−84
	755	98	67	49	27	5	−4	−14	−22	−27	−34	−45	−48	−53	−61	−77	−89
	796	96	63	45	25	+2	−5	−18	−23	−29	−36	−46	−50	−55	−64	−80	−91
	837	110	51	29	7	−9	−18	−27	−32	−36	−43	−52	−57	−62	−73	−89	−105
	878	117	57	37	15	−3	−12	−21	−26	−30	−37	−47	−51	−58	−69	−85	−101
	918	109	57	37	14	−5	−12	−22	−28	−31	−40	−49	−53	−60	−69	−85	−101
	959	111	55	35	15	−3	−14	−22	−28	−31	−37	−47	−51	−60	−67	−83	−99

330	397	207	158	137	113	95	82	67	49	48	24	+1	−58	−99	−130	−157	−173
	412	206	148	123	94	76	65	47	32	29	11	−4	−32	−80	−132	−159	−175
	428	205	140	113	84	66	51	35	22	21	+4	−12	−28	−62	−128	−158	−174
	443	201	132	103	74	58	43	29	14	11	−4	−18	−30	−52	−123	−159	−175
	473	188	123	92	63	45	34	18	+9	+5	−9	−23	−34	−45	−116	−161	−179
	504	177	110	80	53	33	22	11	0	−2	−16	−30	−39	−48	−107	−161	−182
	535	167	100	73	46	28	17	5	−6	−8	−21	−33	−42	−51	−88	−158	−183
	566	164	97	70	43	24	14	+3	−8	−8	−22	−33	−42	−51	−69	−151	−180
	597	155	89	62	37	17	8	−3	−12	−13	−26	−37	−45	−53	−56	−151	−189
	628	149	86	59	34	15	+6	−6	−15	−17	−28	−38	−45	−53	−56	−113	−178
	690	143	78	52	27	9	0	−11		−20	−31	−41	−46	−55	−61	−66	−155
	752	128	69	45	22	+4	−4	−14	−20	−23	−32	−41	−46	−53	−61	−70	−138
	814	121	61	38	16	−2	−11	−20	−27	−29	−38	−48	−53	−62	−70	−82	−136
	876	112	54	33	11	−9	−18	−27	−34	−38	−45	−55	−59	−66	−75	−89	−118
	907	106	50	28	8	−12	−21	−30	−37	−39	−48	−56	−62	−67	−76	−90	−113
	938	108	52	31	9	−11	−20	−29	−36	−38	−47	−55	−61	−66	−75	−89	−111
	969	109	53	30	8	−12	−19	−30	−35	−39	−48	−56	−61	−67	−76	−92	−110
550	560	216	171	171	168	157	149	76	49	42	19	−72	−94	−117	−135	−155	−167
	571	223	167	140	111	88	73	53	33	28	12	−60	−94	−120	−138	−160	−171
	582	220	156	129	99	75	59	39	22	17	+3	−22	−62	−113	−135	−158	−169
	593	207	144	117	86	63	50	31	15	+10	−6	−28	−58	−104	−135	−160	−172
	616	191	126	99	68	44	32	15	+3	−3	−17	−38	−53	−92	−131	−160	−172
	639	184	119	94	63	40	29	13	0	−4	−18	−37	−48	−80	−123	−157	−172
	661	174	109	84	55	32	19	5	−6	−12	−26	−44	−53	−76	−122	−158	−171
	684	173	106	81	50	28	15	+1	−10	−13	−26	−44	−49	−70	−121	−158	−172
	707	164	98	71	42	22	9	−5	−16	−20	−32	−46	−55	−71	−123	−161	−177
	729	160	93	66	39	19	6	−8	−17	−22	−33	−49	−54	−69	−119	−162	−178
	774	148	85	58	31	11	+2	−13	−22	−25	−36	−48	−57	−66	−118	−163	−179
	819	143	78	52	27	5	−4	−16	−25	−29	−40	−52	−59	−68	−107	−161	−182
	864	132	74	51	25	+5	−7	−18	−25	−31	−38	−50	−55	−66	−91	−152	−177
	910	124	66	43	19	−1	−12	−22	−30	−35	−42	−54	−58	−67	−74	−146	−174
	932	119	63	40	16	−2	−11	−23	−31	−34	−43	−54	−59	−66	−66	−139	−170
	955	117	61	37	14	−5	−14	−24	−31	−35	−42	−54	−58	−65	−62	−132	−169
	977	110	60	38	16	−4	−16	−23	−29	−34	−41	−52	−57	−66	−64	−113	−155
800	761	196	136	111	82	59	42	24	4	−3	−21	−112	−133	−153	−158	−173	−180
	774	188	128	103	76	53	36	20	+2	−5	−23	−87	−116	−146	−154	−170	−177
	788	182	118	93	64	43	28	10	−6	−12	−30	−69	−104	−142	−155	−173	−180
	801	180	118	93	64	41	24	+10	−6	−12	−28	−54	−92	−131	−151	−171	−178
	814	162	106	79	50	26	12	−3	−17	−24	−37	−58	−90	−129	−154	−175	−183
	841	165	102	79	52	28	14	+1	−12	−17	−32	−47	−71	−115	−144	−167	−176
	867	150	94	71	42	20	4	−7	−16	−22	−34	−52	−62	−105	−141	−168	−177
	894	140	86	62	35	12	−1	−13	−22	−28	−39	−54	−60	−97	−139	−167	−178
	947	121	69	47	24	4	−7	−20	−27	−32	−41	−54	−57	−79	−132	−170	−179
	973	114	65	45	24	4	−5	−16	−23	−27	−36	−48	−52	−63	−123	−163	−172

TABLE 1—*continued*

(*e*) $M = 2 \cdot 8$

α(degrees)

$10^3 y/s_T$	$10^3 x/c_0$	$-12\cdot44$	$-8\cdot30$	$-6\cdot23$	$-4\cdot15$	$-3\cdot11$	$-2\cdot07$	$-1\cdot04$	0	0	$1\cdot04$	$2\cdot07$	$3\cdot11$	$4\cdot15$	$6\cdot23$	$8\cdot30$	$12\cdot44$
0	100	157	151	129	106	94	87	73	67	65	62	56	50	44	+ 36	+ 28	+ 17
	200	156	115	91	70	56	40	32	25	21	21	15	11	+ 5	− 5	− 14	− 22
	300	156	107	85	62	48	36	31	21	17	17	11	+ 7	− 1	− 10	− 20	− 30
	400	143	100	77	55	42	30	24	10	8	8	+ 2	− 3	− 11	− 19	− 31	− 42
	500	138	95	70	48	35	23	15	3	+ 1	+ 1	− 5	− 11	− 18	− 28	− 38	− 49
	600	123	90	66	43	31	17	9	+ 2	− 2	− 4	− 10	− 16	− 24	− 32	− 41	− 53
	700	113	88	64	43	29	15	7	− 2	− 4	− 8	− 14	− 20	− 24	− 37	− 45	− 56
	750	88	82	64	47	31	15	7	− 6	− 8	− 8	− 14	− 20	− 30	− 37	− 45	− 55
065	148	161	127	104	84	75	61	55	45	41	39	33	26	14	0	− 12	− 56
	193	155	122	98	77	63	49	41	37	33	29	22	16	6	− 6	− 17	− 50
	238	155	114	90	69	55	41	37	24	24	22	14	8	0	− 14	− 23	− 47
	283	152	109	83	62	50	38	30	22	18	16	9	5	3	− 17	− 25	− 36
125	204	168	136	117	97	85	73	67	54	52	52	38	28	5	− 48	− 69	− 87
	224	180	131	108	88	75	63	57	47	43	39	27	18	+ 6	− 12	− 66	− 89
	244	169	127	104	80	67	53	47	35	33	29	18	10	− 2	− 16	− 52	− 84
	265	171	127	104	78	65	53	45	31	29	26	16	+ 6	− 4	− 19	− 39	− 78
	306	152	107	85	64	52	38	29	21	17	13	+ 5	− 3	− 12	− 26	− 36	− 80
	428	162	107	82	58	45	29	21	11	9	6	0	− 8	− 16	− 29	− 37	− 68
	469	148	99	73	50	36	24	16	9	5	+ 1	− 5	− 13	− 23	− 32	− 42	− 60
	510	140	96	73	49	36	22	14	+ 4	+ 2	− 2	− 9	− 15	− 25	− 36	− 44	− 58
	592	129	90	65	43	29	16	8	0	− 4	− 6	− 14	− 20	− 27	− 39	− 49	− 60
	673	112	84	61	39	24	10	+ 2	− 8	−12	−14	− 20	− 25	− 35	− 47	− 54	− 64
	755	91	75	55	34	20	4	− 4	−11	−17	−19	− 25	− 31	− 39	− 50	− 60	− 67
	796	88	73	55	33	18	+ 4	− 4	−12	−16	−20	− 25	− 31	− 41	− 51	− 58	− 66
	837	104	59	36	12	2	− 9	−17	−27	−29	−31	− 37	− 45	− 50	− 62	− 71	− 81
	878	109	64	40	17	5	− 7	−14	−22	−24	−26	− 34	− 40	− 46	− 59	− 67	− 78
	918	101	64	42	21	7	− 7	−13	−20	−22	−26	−32	−40	− 48	− 57	− 67	− 76
	959	103	64	42	19	7	− 5	−13	−24	−24	−24	− 32	− 38	− 48	− 57	− 65	− 76

330	397	209	156	132	111	99	83	67	50	46	32	−3	−44	−73	−108	−122	−131
	412	204	141	116	92	78	63	47	31	29	18	+12	−14	−60	−105	−122	−132
	428	201	136	109	83	69	54	38	24	20	13	+1	−13	−40	−93	−120	−129
	443	194	129	100	73	59	45	31	16	12	+4	−6	−20	−37	−88	−117	−128
	473	188	120	90	65	51	37	23	10	+8	−2	−14	−25	−39	−80	−113	−128
	504	175	106	79	53	40	26	14	+2	−2	−7	−19	−29	−42	−75	−110	−128
	535	166	99	74	46	35	21	9	−3	−5	−11	−20	−30	−42	−69	−108	−125
	566	162	99	72	46	35	21	9	−3	−5	−11	−20	−30	−40	−65	−100	−121
	597	158	91	64	38	27	15	+3	−7	−11	−16	−26	−34	−44	−65	−104	−127
	628	150	87	60	35	23	9	−1	−11	−13	−18	−26	−34	−46	−61	−102	−127
	690	142	83	57	34	22	8	−2	−11	−13	−19	−25	−35	−42	−56	−89	−120
	752	128	73	49	26	14	+2	−7	−15	−17	−21	−29	−35	−44	−54	−67	−104
	814	116	67	43	20	8	−4	−11	−19	−21	−25	−33	−41	−50	−58	−60	−106
	876	104	61	38	16	2	−9	−17	−25	−27	−31	−39	−45	−54	−62	−67	−102
	907	99	58	35	13	1	−11	−18	−28	−30	−32	−40	−48	−55	−63	−69	−100
	938	100	59	36	14	0	−13	−21	−29	−29	−33	−41	−47	−54	−64	−69	−97
	969	101	56	33	11	0	−14	−20	−28	−30	−34	−41	−47	−55	−64	−70	−95
550	560	186	189	187	184	176	107	83		50	41	−18	−46	−77	−106	−117	−123
	571	229	174	147	117	100	80	62	43	35	25	−18	−51	−80	−109	−121	−124
	582	221	164	136	103	86	68	52	31	25	17	−9	−46	−77	−106	−117	−123
	593	211	152	121	93	76	58	44	23	17	+9	−3	−40	−77	−106	−119	−125
	616	193	135	105	74	58	40	29	13	7	−1	−16	−32	−61	−96	−113	−123
	639	186	127	98	69	53	35	22	8	+4	−6	−16	−29	−53	−88	−109	−120
	661	174	117	89	60	42	27	13	+1	−3	−11	−24	−36	−51	−84	−108	−119
	684	172	113	84	56	41	23	11	0	−4	−10	−24	−34	−49	−80	−103	−111
	707	163	104	75	47	32	14	4	−7	−11	−17	−29	−41	−54	−83	−106	−122
	729	156	99	72	44	29	13	+3	−11	−15	−16	−30	−42	−53	−81	−104	−119
	774	147	88	63	37	22	8	−4	−14	−16	−24	−33	−41	−53	−78	−105	−120
	819	136	81	53	30	16	0	−7	−19	−23	−27	−37	−47	−56	−81	−108	−124
	864	126	81	55	30	16	+2	−7	−21	−23	−25	−35	−41	−54	−75	−102	−118
	910	119	74	48	25	9	−5	−14	−24	−26	−30	−38	−46	−55	−79	−106	−119
	932	114	73	47	24	10	−6	−14	−24	−26	−29	−37	−45	−55	−78	−103	−118
	955	115	69	44	20	7	−7	−15	−25	−27	−31	−38	−46	−56	−77	−104	−122
	977	106	71	47	24	10	−4	−11	−25	−27	−25	−35	−41	−52	−72	−99	−114
800	761	199	146	119	89	71	54	38	15	11	−1	−58	−89	−114	−132	−139	−139
	774	189	138	111	83	67	48	32	9	5	−1	−19	−66	−101	−126	−133	−133
	788	181	128	99	71	56	38	24	5	+1	−7	−21	−62	−99	−128	−135	−137
	801	180	129	99	72	56	36	25	+3	−1	−7	−20	−54	−89	−119	−131	−133
	814	161	114	85	57	40	22	13	−5	−11	−17	−30	−54	−87	−119	−133	−134
	841	164	115	87	58	42	26	14	−3	−7	−11	−25	−40	−70	−102	−118	−126
	867	149	106	77	51	36	18	+6	−9	−13	−15	−31	−45	−64	−95	−116	−124
	894	136	97	70	42	27	9	−3	−16	−18	−22	−36	−48	−63	−92	−113	−125
	947	122	82	57	31	18	2	−6	−20	−22	−26	−37	−47	−59	−84	−111	−122
	973	116	78	55	33	20	4	−4	−12	−16	−20	−29	−39	−51	−72	−97	−109

TABLE 2

Values of $10^3 C_p$*: Transition Free, Small Sting Shroud,* $R = 1 \times 10^6/ft$

$M = 2 \cdot 0$

α(degrees)

$10^3 y/s_T$	$10^3 x/c_0$	$-8 \cdot 22$	$-6 \cdot 16$	$-4 \cdot 11$	$-2 \cdot 05$	0	$2 \cdot 05$	$4 \cdot 11$	$6 \cdot 16$	$8 \cdot 22$
0	100	072	72	68	103	95	84	77	+ 62	+ 63
	200	104	93	62	51	33	19	+ 6	− 11	− 8
	300	104	90	55	44	26	9	− 1	− 18	− 18
	400	89	75	44	29	15	+ 2	− 12	− 36	− 36
	500	83	70	42	30	+ 9	− 8	− 21	− 42	− 46
	600	76	66	32	19	− 5	− 19	− 32	− 53	− 54
	700	65	58	24	8	− 16	− 30	− 43	− 68	− 65
	750	48	48	20	4	− 10	− 26	− 39	− 61	− 65
065	148	108	104	79	73	51	34	20	− 3	− 3
	193	101	98	66	55	34	20	7	− 14	− 14
	238	101	91	60	45	27	14	0	− 21	− 21
	283	102	89	61	46	25	11	1	− 23	− 23
125	204	119	115	90	81	59	38	− 2	− 85	− 96
	224	118	108	79	69	45	24	+ 3	− 21	− 73
	244	115	104	73	59	34	14	− 3	− 27	− 45
	265	115	104	70	55	34	+ 14	− 3	− 27	− 28
	306	100	87	55	41	16	− 1	− 21	− 39	− 36
	428	88	74	44	39	14	− 6	− 19	− 40	− 41
	469	85	72	41	29	+ 8	− 9	− 26	− 47	− 48
	510	79	69	35	22	− 2	− 15	− 35	− 53	− 54
	592	78	64	30	17	− 7	− 24	− 37	− 79	− 62
	673	68	61	23	7	− 10	− 27	− 43	− 88	− 69
	755	45	42	11	− 2	− 22	− 36	− 55	− 80	− 75
	796	41	37	7	− 7	− 24	− 41	− 57	− 83	− 76
	837	55	38	5	− 12	− 29	− 49	− 62	− 83	− 92
	878	63	50	12	− 1	− 21	− 42	− 54	− 62	− 84
	918	50	39	2	− 11	− 32	− 52	− 68	− 69	− 84
	959	56	43	9	− 8	− 25	− 45	− 61	− 77	− 88

330	397	153	129	104	84	42	−9	−123	−167	−183
	412	142	114	86	62	24	−10	−107	−178	−187
	428	136	109	77	53	18	−16	−76	−178	−190
	443	128	98	63	42	7	−20	−50	−168	−191
	473	118	91	56	35	+3	−24	−43	−151	−191
	504	109	82	48	29	−5	−29	−49	−118	−182
	535	104	80	45	23	−4	−31	−51	−80	−157
	566		73	39	23	−8	−31	−51	−59	−126
	597	94	66	32	13	−15	−35	−54	−63	−74
	628	87	60	26	9	−18	−42	−58	−69	−56
	690	79	59	25	9	−19	−39	−59	−74	−71
	752	69	49	15	+2	−26	−42	−59	−77	−75
	814	66	45	11	−2	−29	−46	−65	−84	−85
	876	52	35	+1	−12	−36	−56	−72	−94	−92
	907	53	36	−1	−15	−35	−55	−71	−90	−94
	938	52	38	+1	−12	−36	−53	−69	−88	−88
	969	51	34	0	−17	−37	−54	−73	−88	−89
550	560	164	157	118	93	47	−65	−135	−176	−181
	571	156	138	100	70	28	−74	−143	−184	−186
	582	148	130	88	61	20	−25	−138	−179	−185
	593	137	117	79	51	+9	−25	−141	−186	−188
	616	124	103	62	34	−1	−35	−131	−193	−198
	639	111	91	56	28	−3	−34	−110	−189	−194
	661	107	87	45	23	−11	−42	−94	−186	−195
	684	108	91	47	21	−10	−37	−73	−181	−190
	707	99	75	38	15	−19	−42	−69	−180	−196
	729	94	73	35	16	−18	−45	−61	−172	−191
	774	81	61	23	+3	−24	−47	−63	−151	−184
	819	76	55	18	−2	−29	−49	−69	−91	−158
	864	72	55	18	−2	−26	−46	−62	−60	−113
	910	60	43	9	−8	−32	−52	−71	−76	−77
	932	54	40	3	−10	−34	−54	−70	−76	−73
	955	55	38	4	−13	−37	−53	−73	−82	−75
	977	55	38	5	−16	−33	−53	−65	−81	−78
800	761	133	115	74	46	−2	−118	−166	−202	−204
	744	128	111	69	38	−4	−99	−161	−196	−201
	788	119	102	57	32	−9	−87	−166	−202	−204
	801	117	97	55	27	−8	−72	−161	−203	−205
	814	96	79	38	16	−19	−66	−168	−210	−212
	841	99	82	41	18	−16	−43	−156	−205	−211
	867	93	72	35	9	−19	−42	−152	−211	−217
	894	77	60	22	+3	−28	−48	−145	−214	−223
	947	61	47	10	−3	−31	−51	−110	−216	−225
	973	57	44	10	−3	−27	−44	−70	−203	−215

TABLE 3

Values of $10^3 C_p$: Transition Fixed, Large Sting Shroud, $R = 2 \times 10^6/ft$

		(a) $M = 1 \cdot 4$ α(degrees)							(b) $M = 1 \cdot 8$ α(degrees)						
$10^3 y/s_T$	$10^3 x/c_0$	−6·41	−4·27	−2·12	0	2·12	4·27	6·41	−6·36	−4·23	−2·11	0	2·11	4·23	6·36
0	100	89	91	91	72	57	+36	+36	76	80	80	69	59	+49	+39
	200	84	66	47	31	14	−1	−17	66	51	36	20	11	−1	−12
	300	97	71	49	30	+9	−8	−21	79	60	40	22	+12	−4	−17
	400	78	52	28	+8	−11	−28	−47	65	45	25	+5	−8	−24	−37
	500	71	42	14	−8	−27	−45	−64	65	43	21	0	−14	−31	−44
	600	59	30	3	−21	−42	−62	−71	52	30	8	−12	−27	−45	−61
065	148	115	98	81	64	43	+23	0	99	86	71	54	38	17	−1
	193	101	81	62	43	23	0	−20	84	69	52	34	19	+1	−14
	238	95	73	50	30	9	9	−30	77	60	40	22	8	−9	−22
	283	91	67	45	25	6	−13	−32	75	57	37	18	5	−12	−25
125	204	134	122	106	88	59	+28	−105	117	108	93	73	50	+18	−91
	224	110	93	72	50	23	−6	−25	98	79	61	39	18	−8	−31
	244	99	76	52	28	2	−25	−46	84	66	46	24	6	−18	−33
	265	103	79	55	31	+7	−18	−39	88	68	46	25	+6	−17	−31
	306	74	48	24	2	−20	−44	−64	69	48	27	9	−9	−31	−46
	428	93	64	38	+14	−8	−29	−51	83	56	34	12	−6	−24	−39
	469	78	47	21	−3	−23	−45	−66	71	46	23	+3	−16	−36	−51
	510	64	35	+7	−17	−35	−58	−78	59	36	14	−8	−24	−43	−58
	592	53	24	−3	−29	−49	−71	−93	49	26	+4	−18	−34	−53	−70
	673	50	21	−8	−32	−54	−78	−100	40	21	−2	−24	−41	−59	−76
	755	40	14	−15	−40	−61	−85	−109	33	19	−3	−24	−43	−63	−78
	796	33	6	−21	−45	−68	−90	−114	28	13	−9	−27	−46	−66	−83
	837	35	+6	−22	−46	−66	−88	−112	36	9	−14	−33	−51	−71	−88
	878	28	−3	−29	−49	−71	−95	−119	28	+1	−22	−41	−58	−76	−93
	918	14	−13	−39	−59	−80	−102	−104	18	−6	−27	−46	−65	−83	−98
	959	14	−15	−39	−59	−78	−98	−122	18	−4	−27	−47	−62	−81	−96

330	397	184	161	128	89	+22	−155	−222	176	149	117	82	+14	−129	−174
	412	137	106	72	31	−1	−172	−235	134	101	70	32	−5	−132	−182
	428	116	86	51	17	−22	−169	−276	111	80	50	15	−16	−122	−201
	443	108	77	41	+7	−30	−92	−296	103	71	42	+9	−23	−80	−207
	473	93	58	24	−8	−41	−49	−252	89	58	29	−1	−29	−44	−204
	504	87	53	21	−12	−42	−60	−66	81	50	20	−6	−35	−53	−145
	535	78	44	12	−17	−46	−70	−63	75	43	13	−13	−40	−59	−47
	566	70	36	+6	−25	−51	−75	−82	68	36	9	−16	−39	−61	−56
	597	64	28	−3	−32	−59	−83	−95	61	31	4	−19	−43	−65	−70
	628	60	28	−5	−32	−58	−83	−99	59	30	+4	−21	−45	−65	−75
	690	48	17	−15	−41	−66	−89	−109	51	20	−6	−28	−50	−70	−83
	752	41	+12	−18	−42	−66	−88	−109	43	14	−11	−31	−51	−71	−85
	814	28	−3	−30	−54	−76	−98	−122	35	6	−17	−37	−57	−79	−96
	876	28	−3	−30	−54	−76	−100	−122	29	+1	−22	−41	−61	−80	−96
	907	28	−3	−30	−52	−75	−99	−122	26	−1	−24	−44	−49	−81	−98
	938	19	−10	−35	−58	−78	−100	−122	23	−4	−26	−46	−65	−83	−100
	969	14	−13	−37	−58	−76	−99	−122	21	−6	−27	−46	−65	−83	−100
550	571	144	115	76	24	−151	−221	−283	129	101	66	11	−88	−173	−212
	582	127	91	50	+2	−85	−226	−286	120	88	51	10	−54	−176	−213
	593	117	81	40	−6	−54	−243	−295	112	78	45	+3	−44	−185	−217
	616	98	62	23	−22	−54	−273	−325	94	63	26	−13	−46	−190	−229
	639	86	50	+11	−29	−63	−267	−358	84	51	19	−16	−49	−178	−239
	661	72	37	−1	−39	−74	−190	−375	71	41	10	−24	−56	−146	−245
	684	72	37	+1	−35	−69	−81	−366	70	38	6	−26	−54	−98	−247
	707	66	30	−6	−40	−71	−54	−318	65	33	+3	−29	−56	−59	−245
	729	60	25	−11	−44	−76	−74	−218	56	26	−4	−34	−57	−59	−238
	774	49	14	−18	−51	−80	−93	−83	48	18	−9	−36	−61	−74	−136
	819	41	11	−22	−52	−78	−97	−97	46	14	−12	−39	−63	−80	−61
	864	37	+4	−23	−51	−76	−95	−105	38	13	−12	−39	−59	−78	−78
	910	30	−1	−30	−54	−78	−98	−112	30	5	−18	−43	−62	−81	−87
	932	25	−4	−32	−56	−78	−100	−117	26	+1	−22	−44	−62	−81	−88
	955	23	−6	−33	−54	−73	−95	−114	25	0	−24	−44	−62	−81	−88
	977	16	−10	−33	−54	−74	−97	−114	20	−2	−25	−47	−64	−83	−93
800	761	120	86	45	−13	−177	−247	−301	112	81	43	−21	−150	−196	−228
	774	91	55	16	−35	−199	−260	−318	90	61	26	−24	−150	−198	−228
	788	83	49	8	−40	−211	−264	−320	82	52	17	−27	−141	−203	−235
	801	79	45	+4	−38	−207	−269	−320	75	47	15	−28	−119	−206	−235
	814	70	36	−1	−42	−179	−288	−324	68	39	7	−31	−95	−210	−237
	841	60	28	−8	−45	−80	−318	−344	60	30	+1	−34	−57	−225	−247
	867	52	20	−14	−47	−55	−332	392	45	22	−7	−38	−57	−230	−263
	894	41	+12	−18	−49	−66	−313	−418	41	16	−11	−39	−61	−225	−276
	947	18	−6	−28	−47	−68	−144	−419	26	3	−19	−41	−61	−156	−277
	973	11	−6	−23	−42	−61	−85	−382	20	3	−15	−34	−52	−63	−270

TABLE 3—*continued*

$10^3y/s_T$	$10^3x/c_0$	(c) $M = 2{\cdot}0$ α(degrees)							(d) $M = 2{\cdot}4$ α(degrees)						
		−6·33	−4·22	−2·10	0	2·10	4·22	6·33	−6·28	−4·18	−2·09	0	2·09	4·18	6·28
0	100	74	76	76	64	51	+39	+31	74	74	77	68	58	+44	+35
	200	70	52	30	13	+3	−10	−20	70	54	33	18	9	0	−14
	300	78	56	31	+12	0	−15	−23	76	55	33	17	+6	−10	−20
	400	63	12	19	−1	−13	−31	−42	64	42	23	+3	−8	−24	−36
	500	64	12	17	−3	−17	−35	−49	61	38	17	−1	−12	−30	−41
	600	53	31	6	−16	−30	−50	−62	48	32	7	−13	−24	−36	−49
065	148	102	87	65	45	31	+9	−9	98	84	62	44	32	16	−6
	193	88	70	46	26	+13	−7	−21	87	73	48	28	16	+3	−13
	238	79	58	34	14	0	−18	−32	76	57	37	19	5	−11	−26
	283	76	54	31	11	−1	−21	−33	76	57	35	17	5	−11	−26
125	204	119	107	86	64	42	+10	−77	120	102	84	65	43	+15	−57
	224	102	80	55	31	13	−17	−38	98	82	57	35	17	−4	−29
	244	88	68	41	20	+3	−26	−39	89	71	48	26	10	−11	−31
	265	89	67	39	17	0	−25	−40	88	68	43	22	+8	−16	−34
	306	72	48	23	1	−11	−36	−48	73	57	32	10	−4	−20	−38
	428	78	53	25	+3	−11	−32	−44	73	51	25	+3	−11	−25	−40
	469	69	44	17	−5	−17	−40	−54	59	42	15	−5	−17	−32	−46
	510	62	38	11	−11	−24	−48	−59	57	39	12	−7	−20	−34	−49
	592	51	28	+3	−19	−34	−56	−68	46	28	+5	−16	−27	−41	−57
	673	42	22	−5	−27	−40	−62	−76	36	20	−3	−23	−33	−50	−64
	755	40	25	−1	−24	−38	−61	−73	35	27	0	−20	−32	−45	−61
	796	37	22	−3	−27	−37	−62	−74	33	24	−1	−21	−33	−46	−62
	837	43	18	−11	−32	−46	−68	−79	32	14	−13	−31	−43	−57	−72
	878	35	11	−16	−37	−49	−73	−84	26	9	−16	−34	−47	−61	−75
	918	28	6	−21	−42	−53	−76	−86	21	7	−20	−38	−50	−61	−75
	959	25	5	−22	−42	−57	−77	−91	22	4	−19	−37	−49	−66	−78

330	397	168	140	103	44	+12	−127	−162	159	134	101	47	+17	−96	−135
	412	128	98	63	26	−8	−118	−169	125	99	61	24	−3	−78	−137
	428	106	79	44	9	−20	−107	−180	106	79	44	13	−15	−71	−137
	443	100	70	36	+4	−24	−76	−182	99	68	35	+7	−22	−61	−136
	473	88	58	25	−6	−29	−53	−175	83	59	25	−2	−25	−50	−125
	504	81	51	17	−13	−33	−56	−144	74	47	15	−10	−31	−53	−113
	535	74	44	12	−17	−37	−60	−79	68	41	11	−14	−34	−53	−96
	566	70	40	8	−21	−38	−63	−53	60	37	7	−18	−34	−54	−77
	597	62	31	+1	−26	−41	−66	−66	53	30	2	−22	−39	−56	−65
	628	59	29	−1	−26	−43	−67	−72	51	29	+1	−22	−38	−55	−62
	690	51	22	−8	−31	−46	−70	−80	43	22	−6	−28	−42	−58	−67
	752	46	18	−11	−32	−46	−69	−78	37	18	−7	−29	−41	−56	−65
	814	40	13	−15	−37	−50	−76	−86	31	13	−12	−33	−48	−62	−75
	876	36	11	−17	−39	−53	−76	−88	28	9	−16	−36	−50	−63	−77
	907	33	8	−19	−41	−54	−78	−89	26	7	−18	−38	−50	−65	−77
	938	31	6	−21	−44	−56	−78	−89	23	7	−20	−39	−52	−65	−77
	969	30	3	−24	−46	−56	−79	−91	21	5	−22	−39	−52	−65	−79
550	571	129	98	58	11	−73	−161	−190	123	98	59	18	−55	−120	−150
	582	121	91	50	+5	−47	−163	−191	116	90	50	11	−25	−107	−148
	593	112	79	42	0	−42	−166	−195	107	77	42	+6	−26	−101	−148
	616	95	62	23	−14	−46	−163	−200	89	60	25	−7	−36	−93	−145
	639	87	53	18	−19	−46	−151	−203	82	57	21	−11	−38	−84	−139
	661	74	44	8	−25	−50	−120	−205	72	45	11	−19	−44	−82	−141
	684	70	40	7	−27	−52	−101	−201	66	42	8	−21	−44	−76	−139
	707	67	37	+2	−30	−54	−72	−201	61	36	+4	−24	−48	−76	−139
	729	60	30	−3	−34	−55	−65	−200	56	31	−1	−28	−49	−75	−139
	774	54	25	−8	−37	−55	−71	−174	49	25	−7	−30	−49	−69	−132
	819	48	20	−12	−39	−58	−78	−59	41	19	−11	−36	−54	−70	−123
	864	45	22	−10	−37	−55	−76	−66	40	17	−10	−33	−49	−69	−105
	910	39	14	−16	−41	−58	−80	−80	33	12	−15	−38	−52	−72	−86
	932	39	12	−17	−40	−55	−77	−77	33	13	−14	−37	−49	−67	−73
	945	35	10	−17	−40	−55	−77	−78	31	11	−16	−37	−51	−66	−67
	977	29	8	−20	−42	−57	−77	−84	29	6	−16	−37	−49	−69	−69
800	761	112	79	35	−20	−136	−183	−206	100	70	36	−10	−106	−148	−165
	774	94	65	27	−18	−126	−183	−205	91	63	29	−10	−90	−142	−164
	788	88	58	17	−23	−115	−187	−209	83	57	21	−17	−74	−142	−167
	801	83	54	16	−25	−99	−189	−209	81	51	19	−15	−58	−131	−165
	814	75	46	9	−29	−81	−188	−210	73	46	12	−20	−50	−118	−161
	841	67	39	+5	−30	−57	−193	−215	66	40	9	−23	−46	−114	−158
	867	56	31	−3	−36	−55	−192	−222	57	30	+3	−26	−49	−109	−159
	894	50	23	−9	−39	−58	−185	−227	48	27	−4	−31	−52	−104	−155
	947	35	12	−17	−40	−57	−154	−228	34	13	−12	−33	−53	−87	−153
	973	30	10	−13	−37	−52	−91	−216	31	15	−12	−32	−48	−71	−144

TABLE 3—*continued*

(*e*) $M = 2 \cdot 8$

α(degrees)

$10^3 y/s_T$	$10^3 x/c_0$	$-6 \cdot 23$	$-4 \cdot 15$	$-2 \cdot 07$	0	$2 \cdot 07$	$4 \cdot 15$	$6 \cdot 23$
0	100	65	65	67	63	49	41	+ 35
	200	69	49	37	27	5	+ 1	− 11
	300	70	52	36	24	+ 2	− 6	− 16
	400	60	40	24	12	− 10	− 18	− 28
	500	57	37	21	9	− 13	− 23	− 31
	600	48	30	14	2	− 20	− 24	− 38
065	148	96	78	62	52	26	20	− 2
	193	82	64	50	38	+ 12	+ 6	− 12
	238	72	54	24	24	0	− 8	− 22
	283	70	50	34	20	− 2	− 8	− 22
125	204	111	99	83	67	39	19	− 37
	224	98	74	58	42	14	+ 2	− 24
	244	88	70	52	36	8	− 4	− 24
	265	85	63	45	29	+ 1	− 11	− 27
	306	72	52	34	20	− 6	− 14	− 34
	428	68	44	26	12	− 12	− 20	− 36
	469	59	35	19	3	− 19	− 25	− 41
	510	56	36	20	+ 6	− 18	− 24	− 40
	592	48	30	12	0	− 24	− 30	− 46
	673	37	21	7	− 5	− 31	− 37	− 51
	755	36	24	10	− 2	− 26	− 30	− 48
	796	35	23	+ 11	− 1	− 25	− 31	− 47
	837	36	12	− 4	− 18	− 40	− 46	− 62
	878	30	10	− 6	− 22	− 44	− 50	− 64
	918	26	8	− 8	− 20	− 42	− 46	− 64
	959	25	7	− 7	− 21	− 43	− 55	− 65

330	397	150	122	94	53	− 3	− 73	−114
	412	122	90	63	33	+ 5	− 51	−110
	428	104	75	47	21	− 11	− 47	−100
	443	94	64	38	12	− 20	− 44	− 95
	473	84	54	28	+ 6	− 26	− 42	− 87
	504	75	43	21	− 1	− 29	− 45	− 84
	535	68	38	16	− 2	− 32	− 46	− 77
	566	64		16	− 4	− 32	− 42	− 71
	597	58	30	8	− 12	− 36	− 46	− 73
	628	55	27	7	− 11	− 35	− 47	− 68
	690	49	23	+ 3	− 13		− 45	− 63
	752	42	18	0	− 16	− 38	− 44	− 58
	814	37	13	− 7	− 21	− 43	− 49	− 65
	876	30	10	− 8	− 22	− 46	− 52	− 66
	907	30	8	− 8	− 22	− 44	− 52	− 66
	938	28	6	− 10	− 24	− 46	− 52	− 66
	969	26	6	− 10	− 24	− 46	− 50	− 66
550	571	127	99	72	38	− 34	− 77	−113
	582	121	91	63	33	− 21	− 73	−110
	593	111	81	53	25	− 13	− 69	−108
	616	92	64	38	14	− 26	− 58	− 99
	639	86	56	32	+ 8	− 30	− 50	− 91
	661	75	47	23	− 1	− 35	− 51	− 90
	684	71	43	19	− 3	− 35	− 49	− 86
	707	65	37	13	− 9	− 41	− 53	− 88
	729	59	33	11	− 11	− 43	− 53	− 86
	774	53	25	+ 5	− 15	− 43	− 53	− 86
	819	44	18	− 2	− 20	− 48	− 58	− 89
	864	39	19	− 1	− 17	− 43	− 55	− 82
	910	32	12	− 6	− 22	− 47	− 58	− 85
	932	35	13	− 5	− 21	− 47	− 53	− 82
	955	33	11	− 7	− 21	− 48	− 55	− 82
	977	31	13	− 3	− 19	− 43	− 57	− 76
800	761	101	73	49	13	− 76	−106	−136
	774	95	71	47	15	− 39	− 88	−124
	788	88	60	34	8	− 34	− 91	−129
	801	84	58	34	8	− 32	− 85	−127
	814	76	50	28	4	− 36	− 79	−119
	841	71	47	23	+ 1	− 37	− 69	−106
	867	60	36	16	− 4	− 42	− 62	− 99
	894	50	30	10	− 12	− 46	− 58	− 93
	947	39	19	1	− 15	− 47	− 59	− 88
	973	37	19	3	− 13	− 41	− 51	− 80

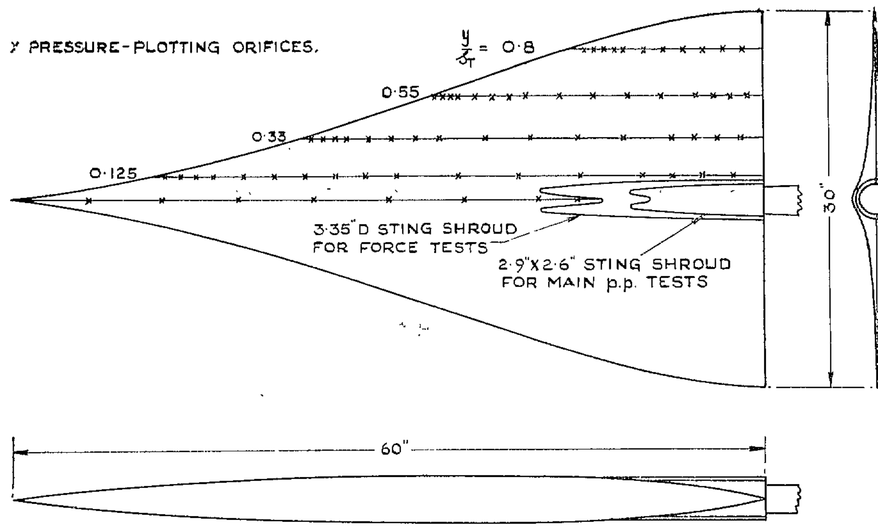

FIG. 1. General arrangement of model.

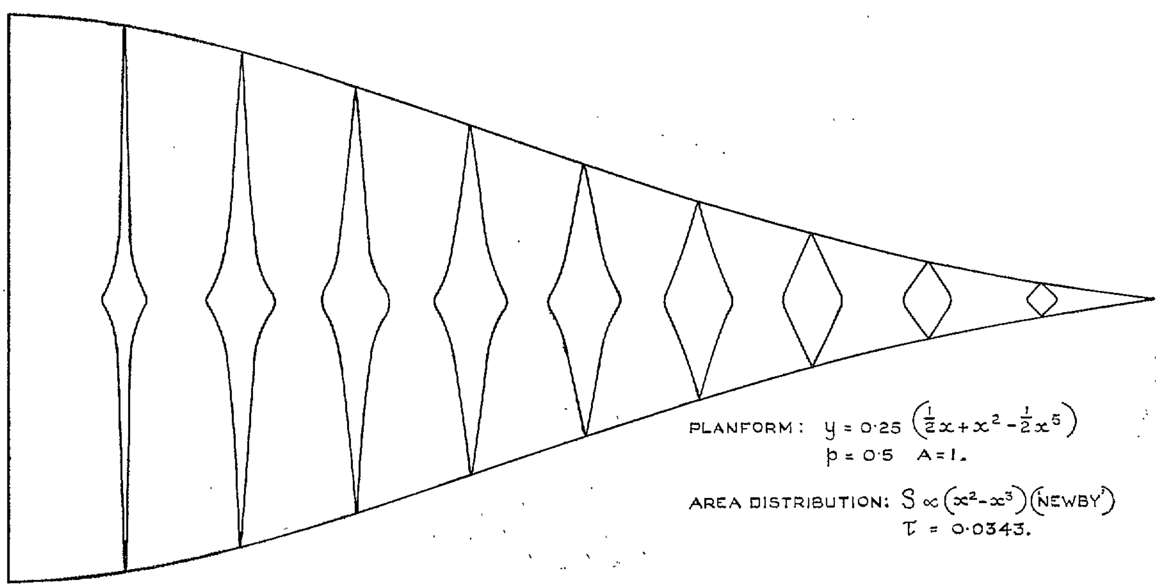

FIG. 2. Planform and cross-section shapes.

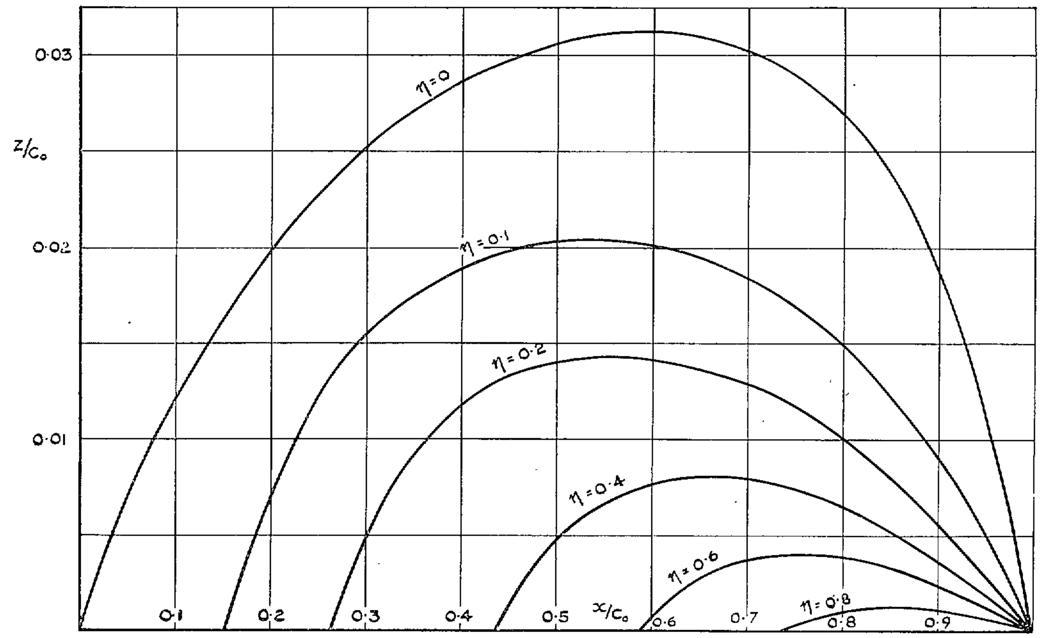

FIG. 3. Chordwise section shapes.

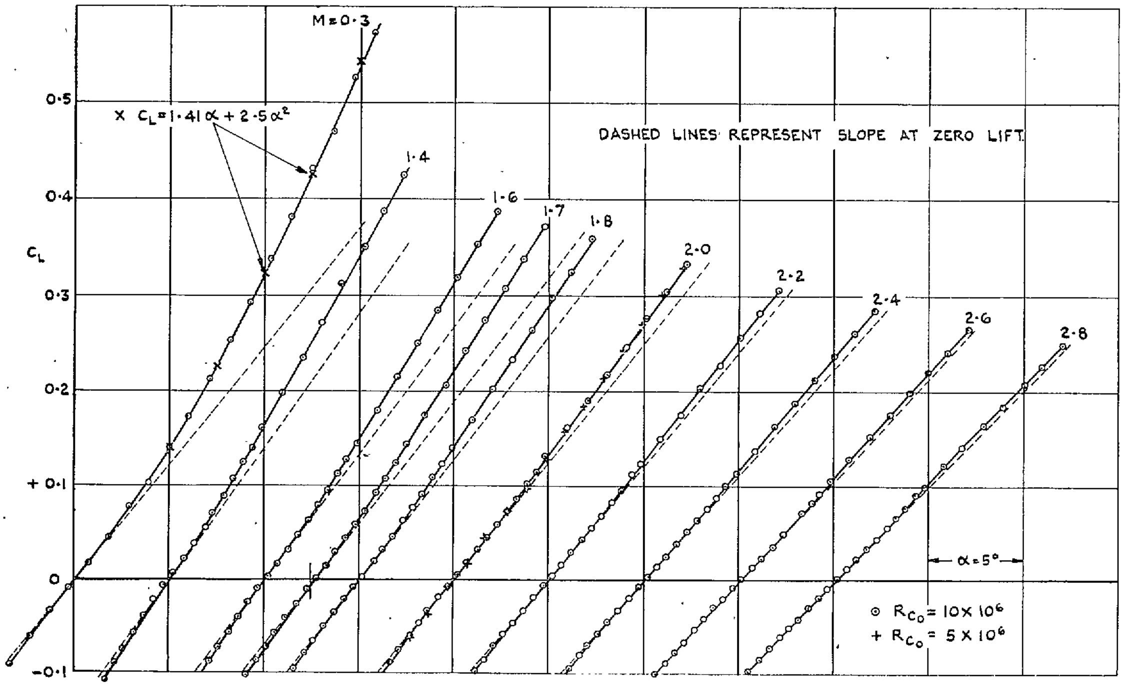

FIG. 4. C_L vs. α at various Mach numbers.

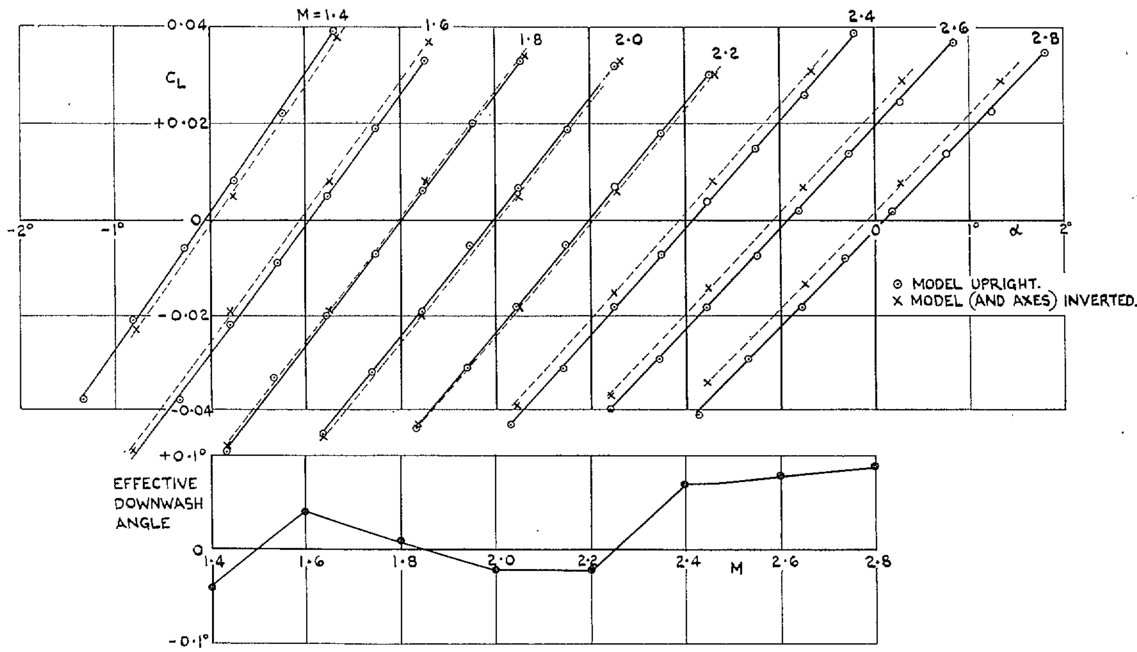

FIG. 5. Lift curves with model inverted, and effective downwash.

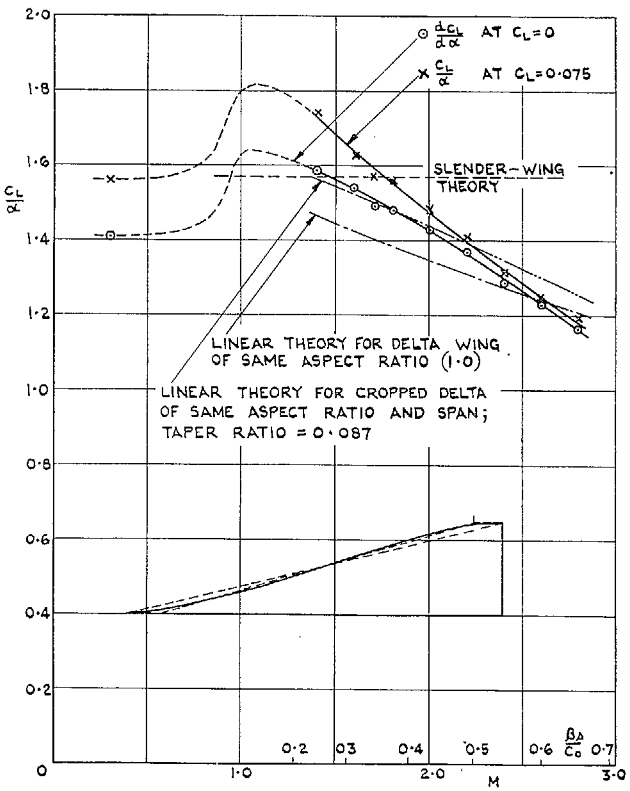

FIG. 6. Variation of C_L/α with Mach number. ($C_L = 0$ and $C_L = 0{\cdot}075$.)

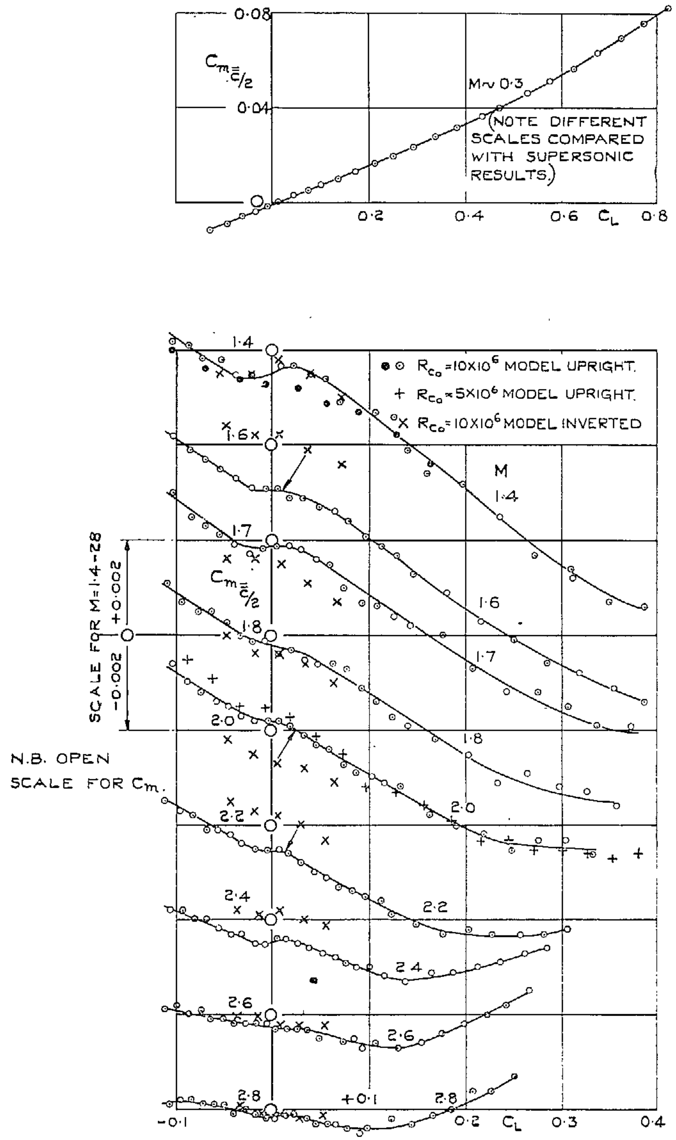

FIG. 7. C_m vs. C_L at various Mach numbers.

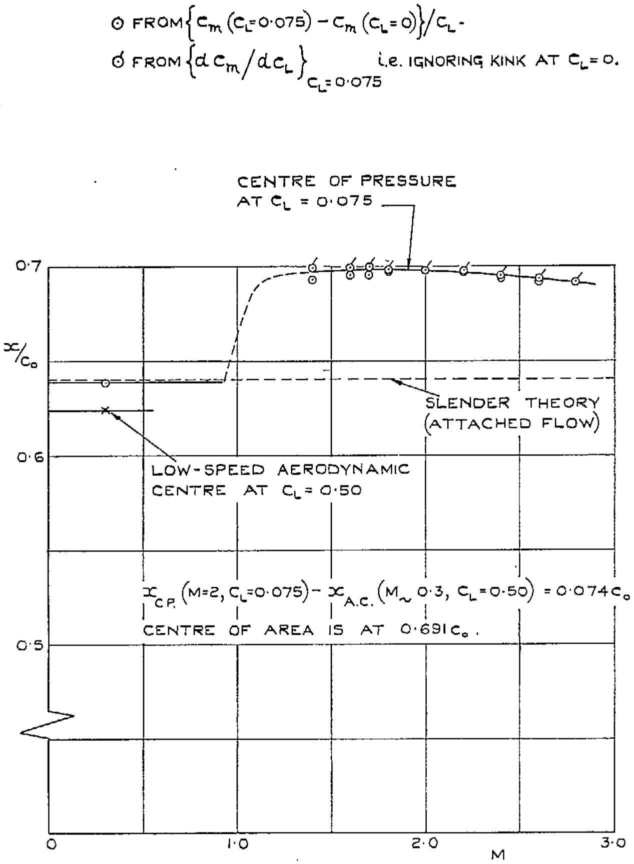

FIG. 8. Centre of pressure and aerodynamic centre.

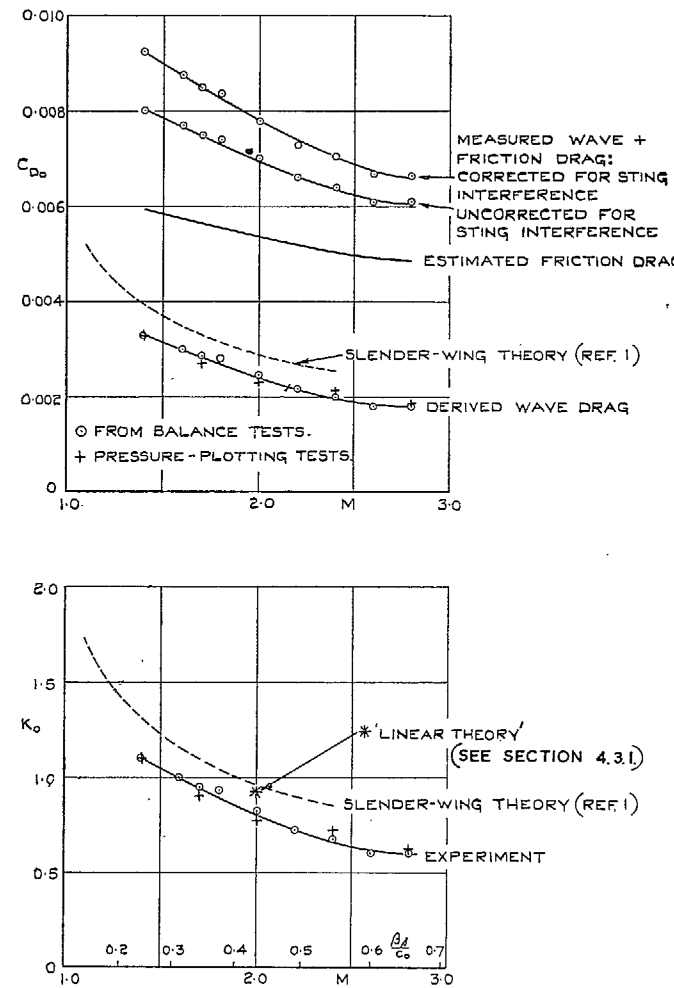

FIG. 9. Zero-lift drag.

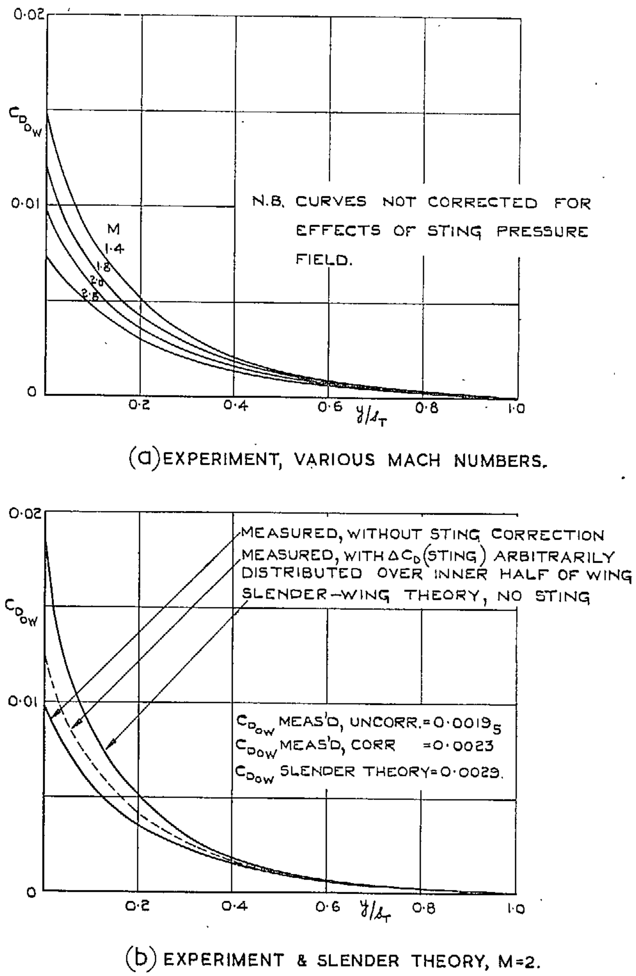

FIG. 10. Spanwise distribution of normal pressure drag at zero lift.

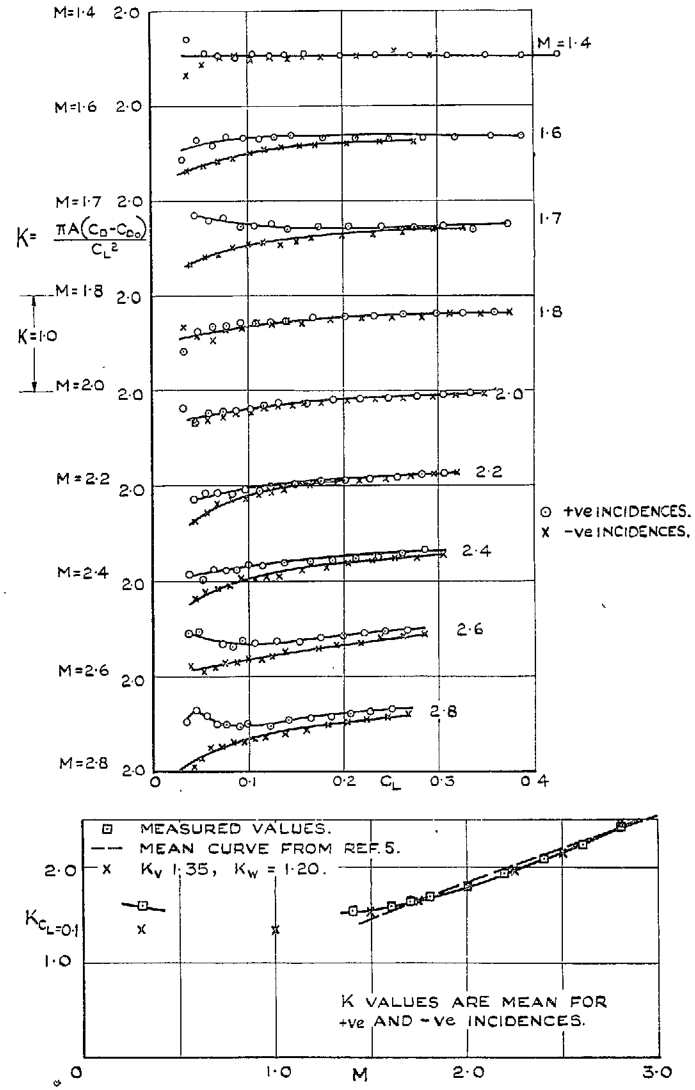

FIG. 11. Lift-dependent drag.

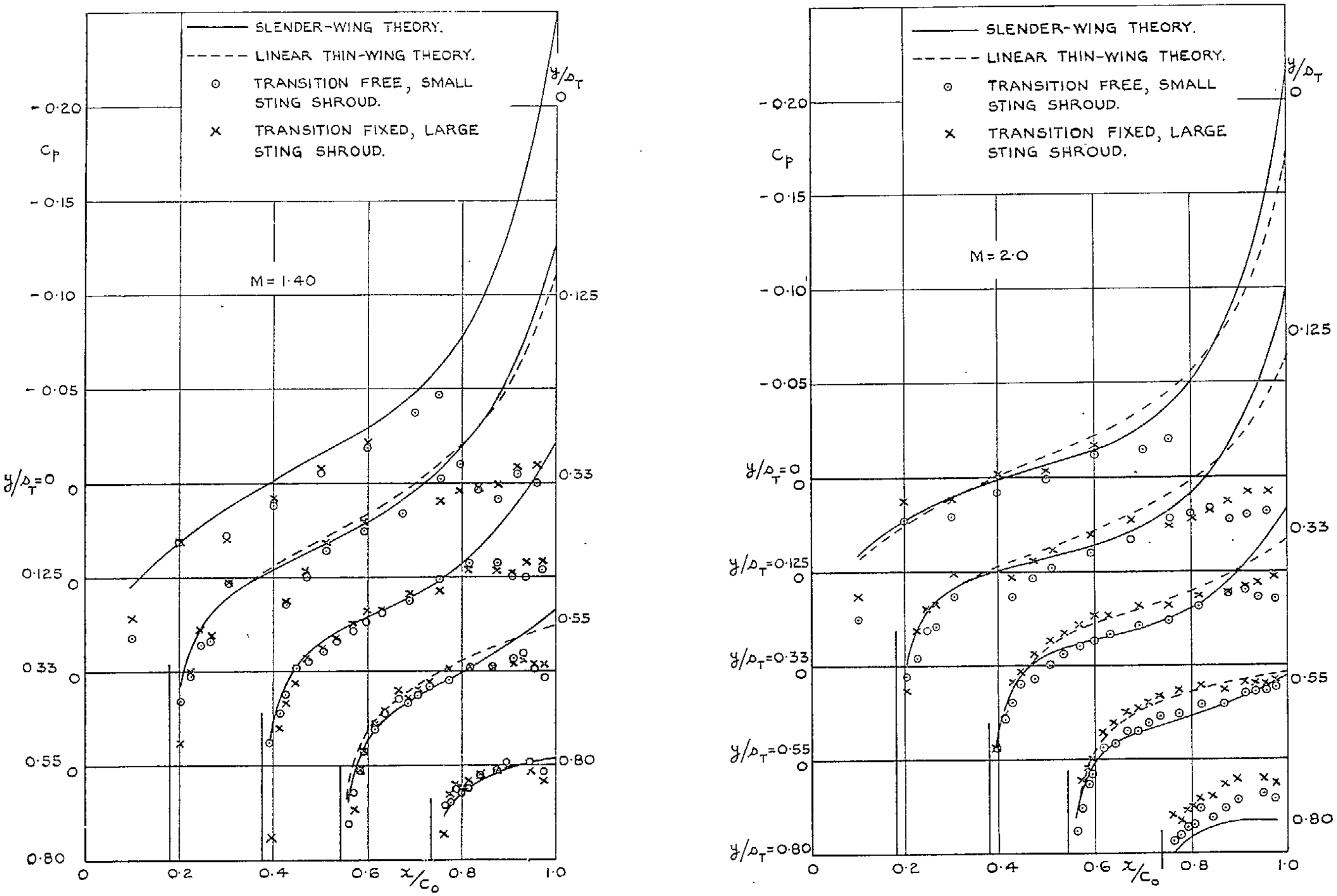

(a) $M = 1{\cdot}4$.

(b) $M = 2{\cdot}0$.

FIG. 12. Chordwise pressure distributions at $\alpha = 0$.

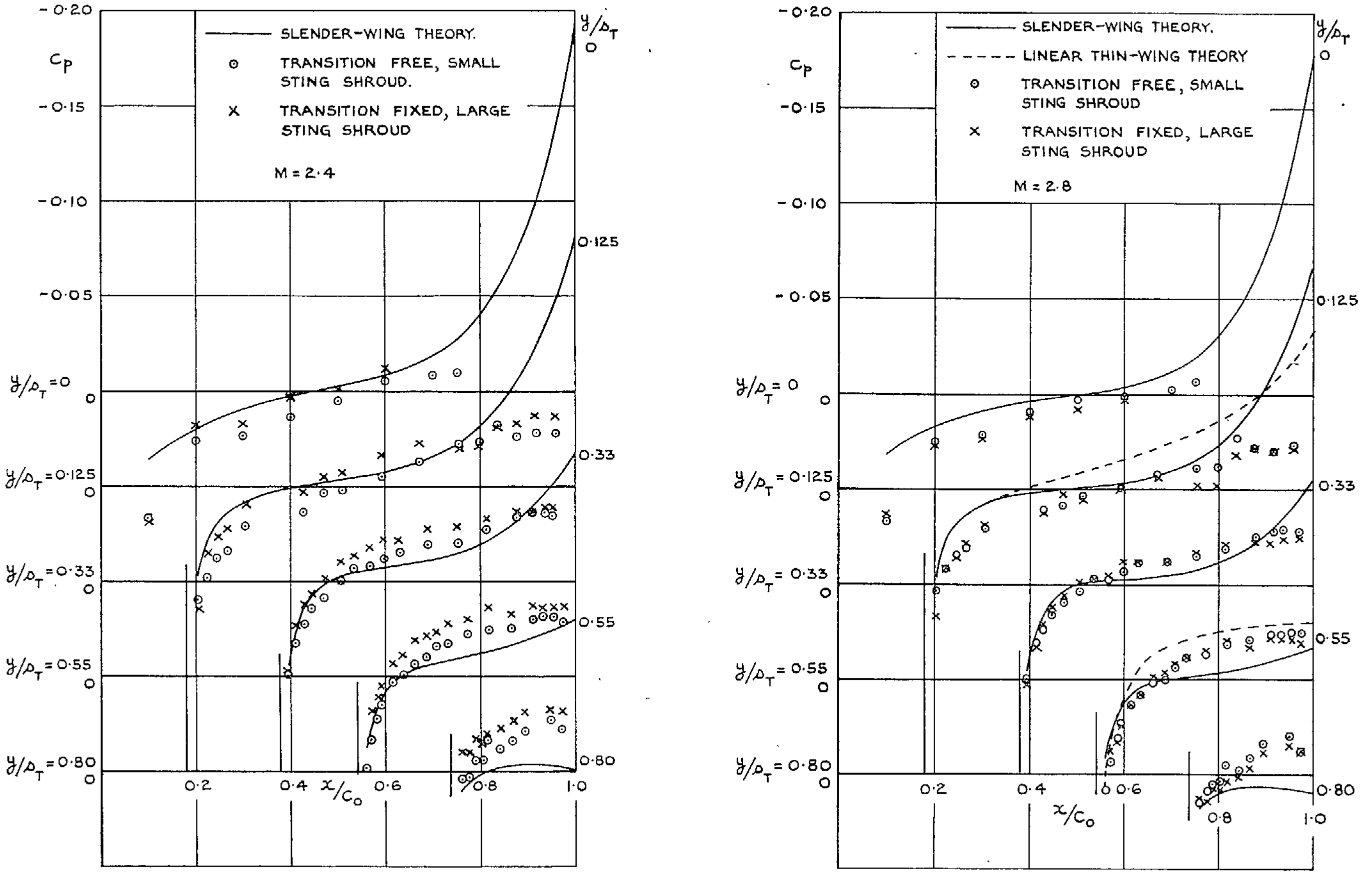

(c) $M = 2{\cdot}4$. (d) $M = 2{\cdot}8$.

FIG. 12. Chordwise pressure distributions at $\alpha = 0$.

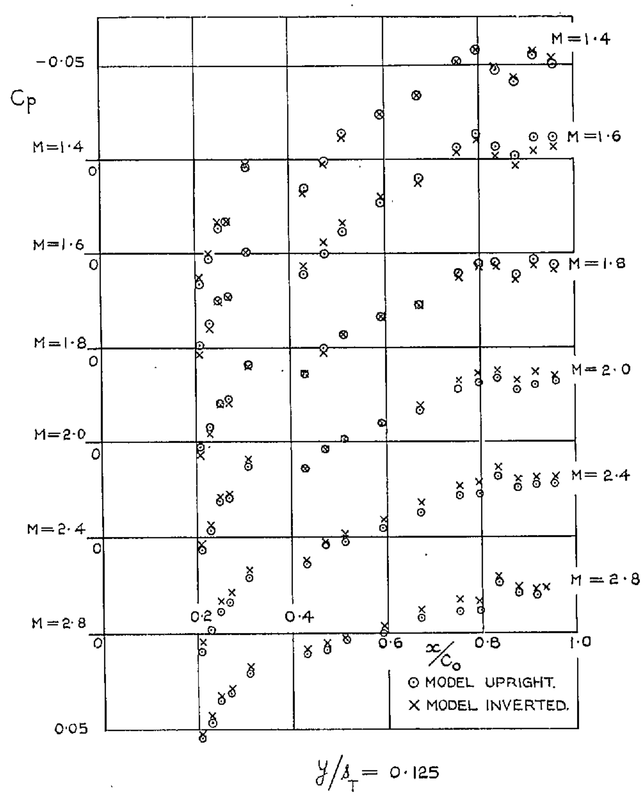

FIG. 13. Effect of inverting model on pressure distributions at $\alpha = 0$, $y/s_T = 0 \cdot 125$.

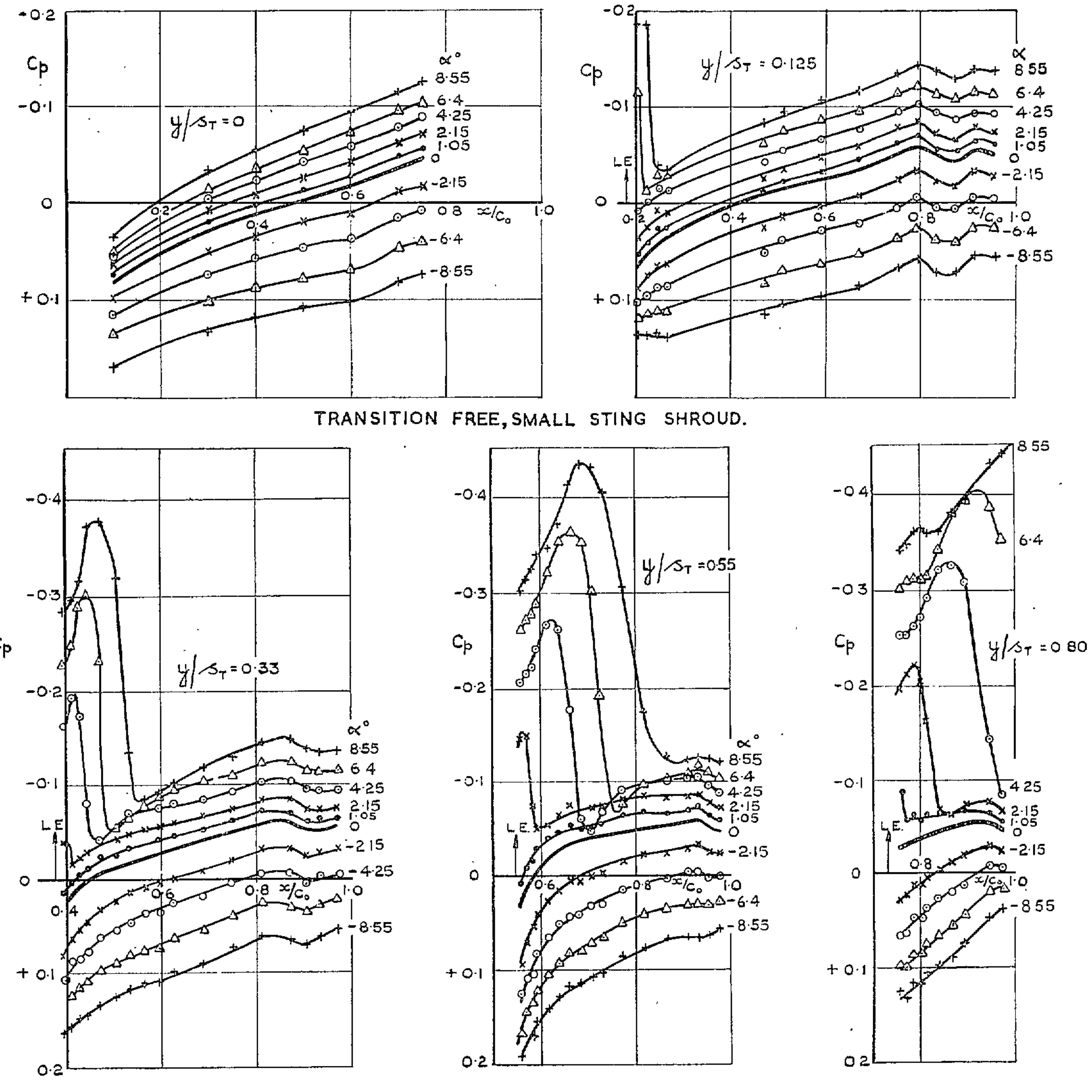

$M = 1{\cdot}4.$

FIG. 14a. Chordwise pressure distributions at various incidences.

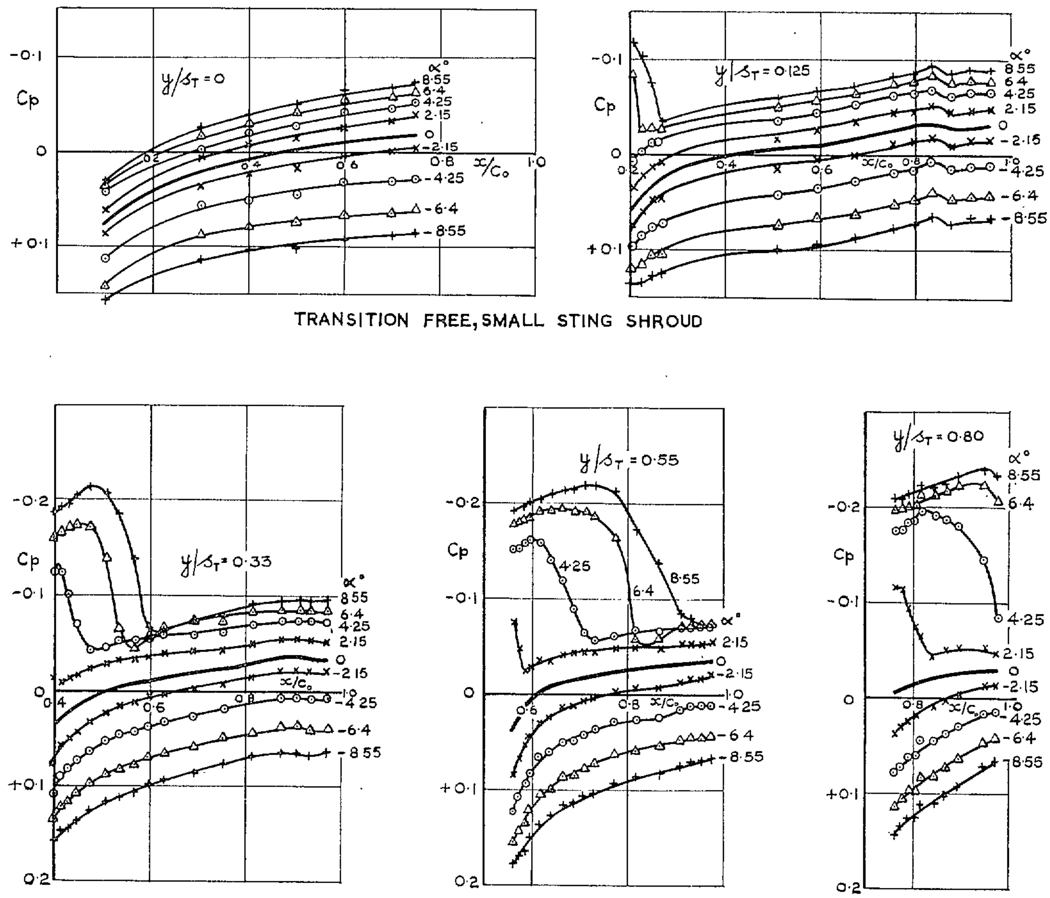

$M = 2 \cdot 0.$

FIG. 14b. Chordwise pressure distributions at various incidences.

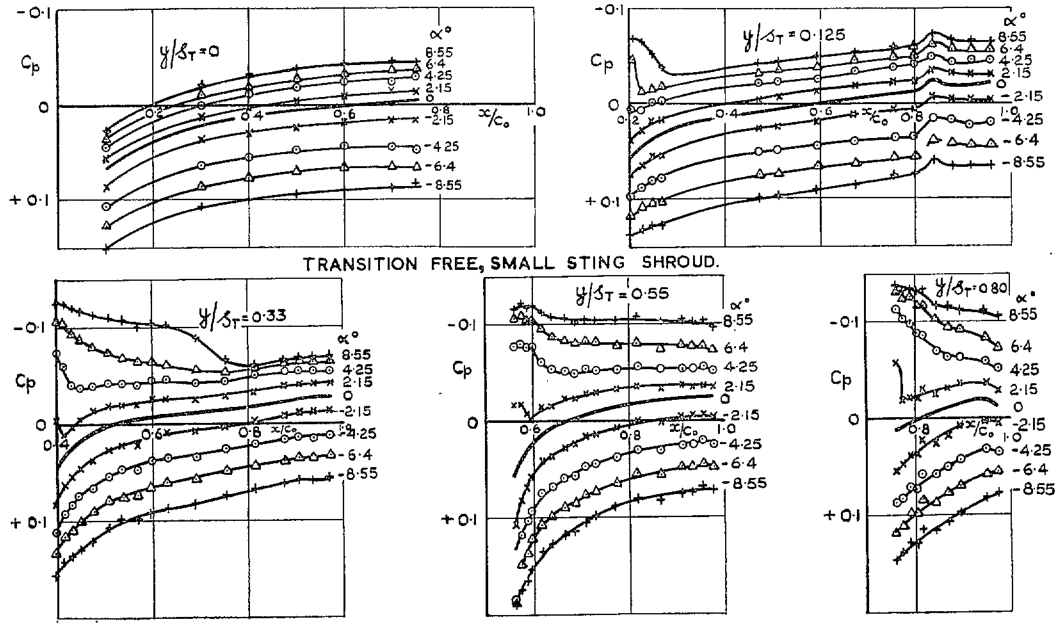

$M = 2{\cdot}8.$

FIG. 14c. Chordwise pressure distributions at various incidences.

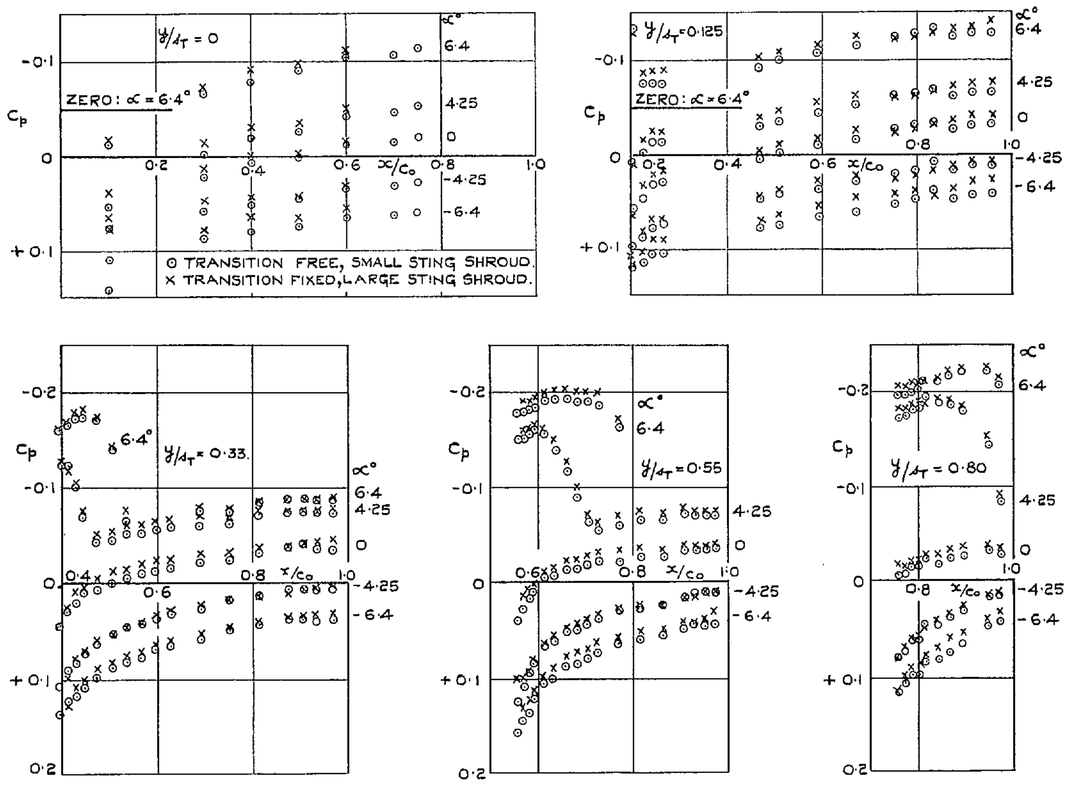

FIG. 15. Effect of transition fixing and larger sting shroud on pressure distributions at $M = 2$.

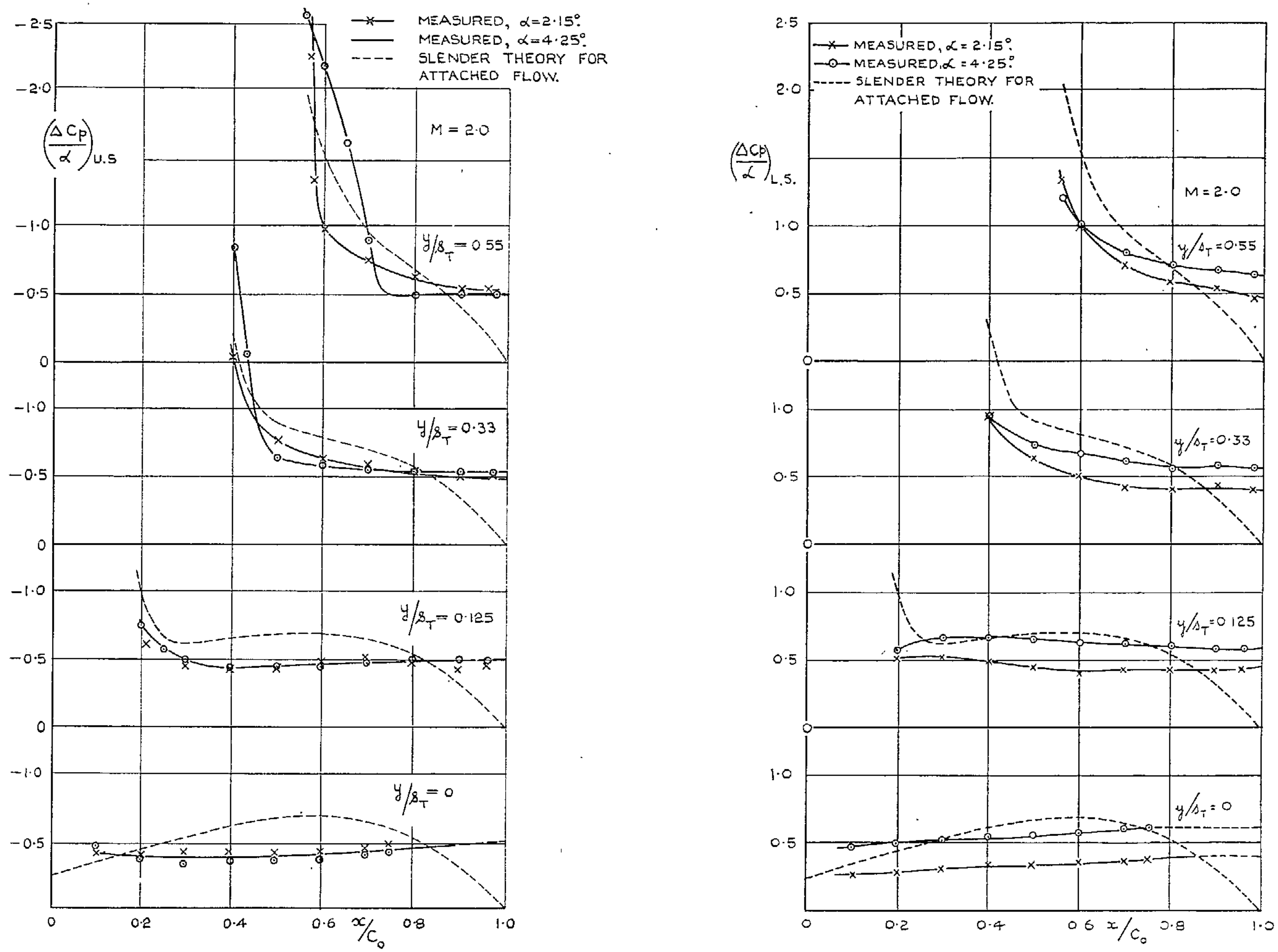

(a) Upper surface, $M = 2$.

(b) Lower surface, $M = 2$.

FIG. 16. Surface pressure increments due to lift.

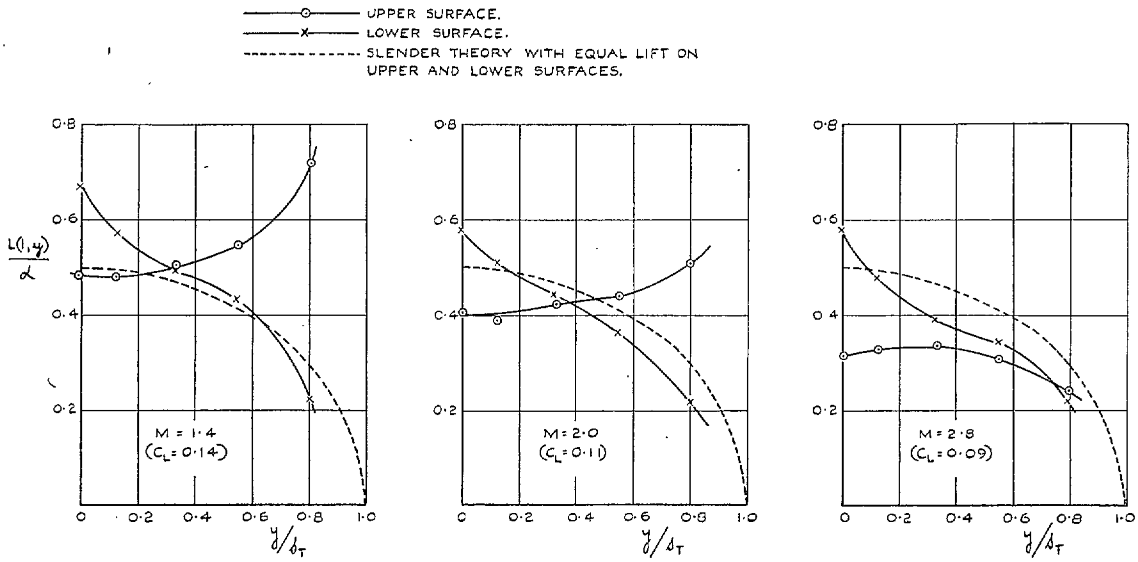

FIG. 17. Contributions of upper and lower surfaces to total chord load at $\alpha = 4 \cdot 25°$.

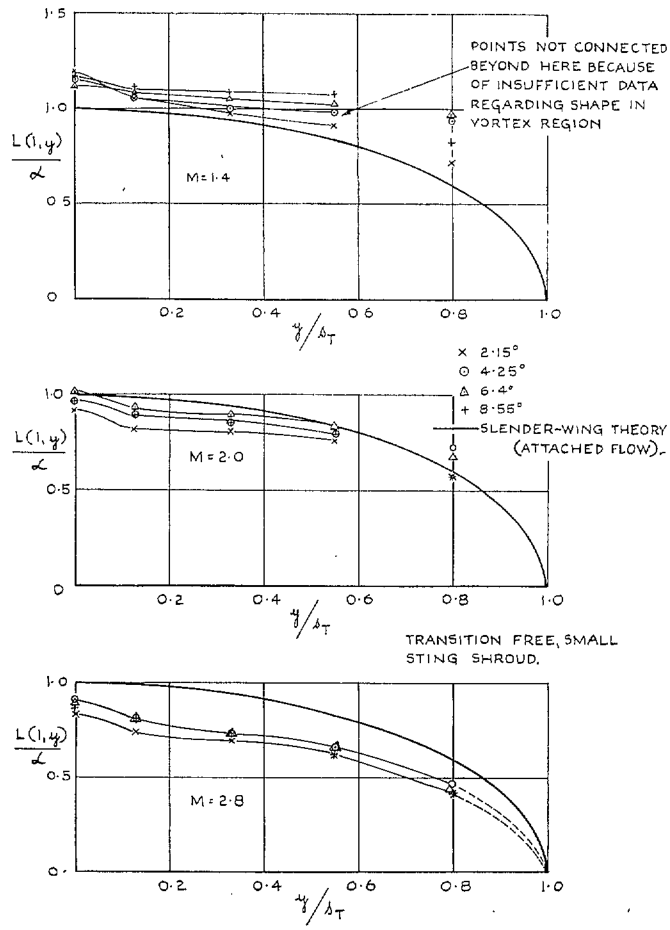

FIG. 18. Spanwise distributions of chord load at various Mach numbers and incidences.

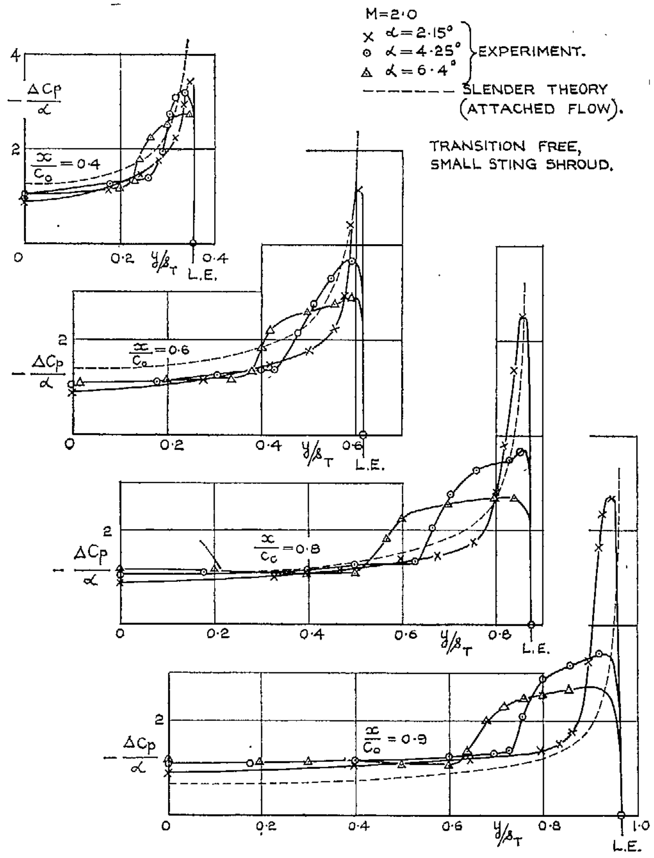

FIG. 19. Spanwise distributions of $\Delta C_p/\alpha$ at various x/C_0: variation with incidence at $M = 2$.

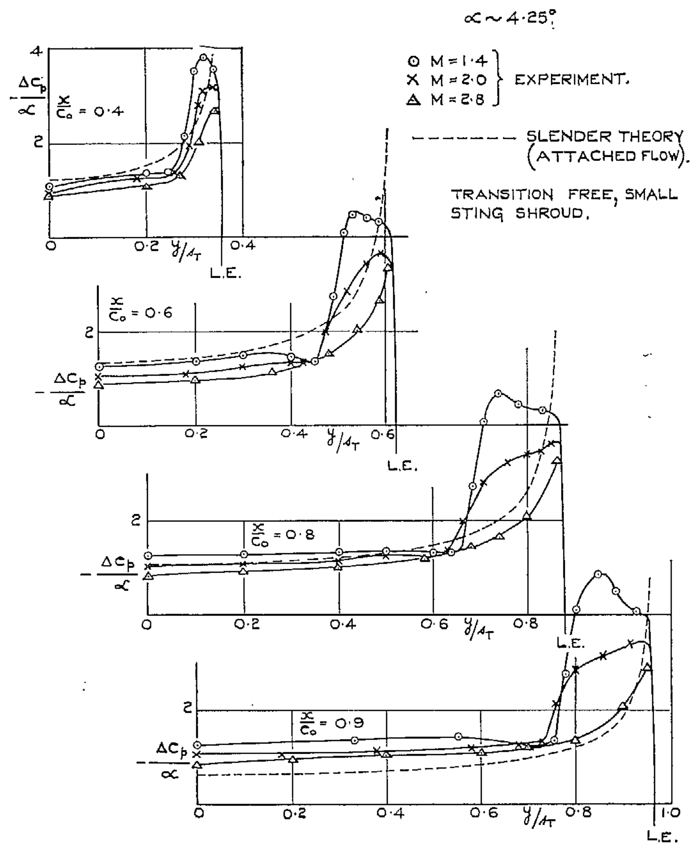

FIG. 20. Spanwise distributions of $\Delta C_p/\alpha$ at various x/C_0: variation with Mach number at $\alpha \sim 4{\cdot}25°$.

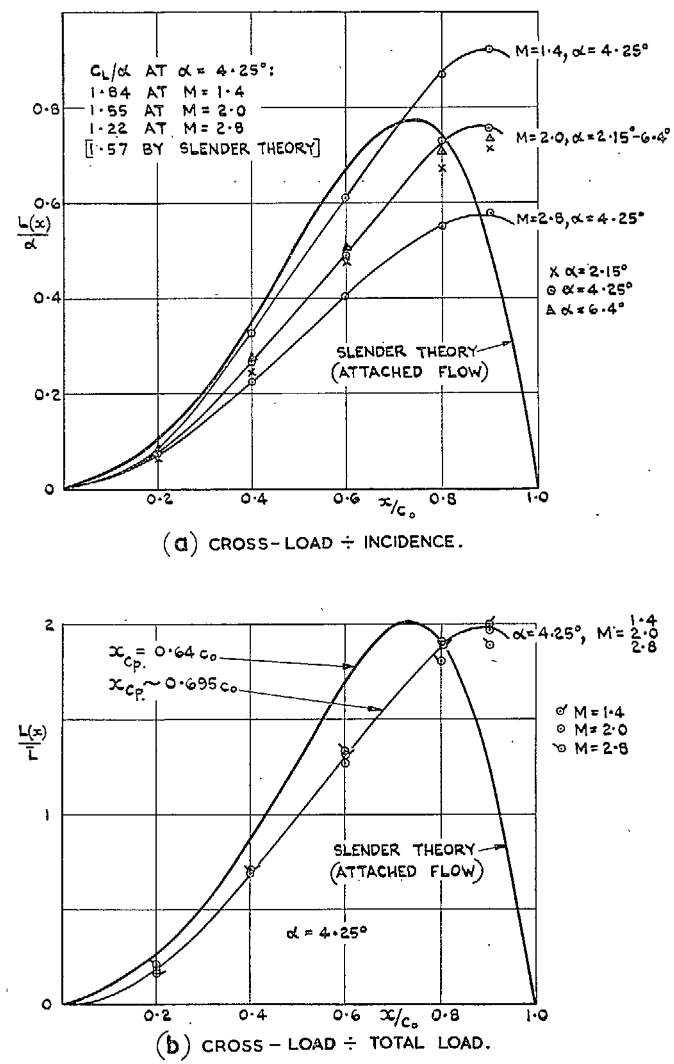

FIG. 21. Cross-load distributions for various Mach numbers and incidences.

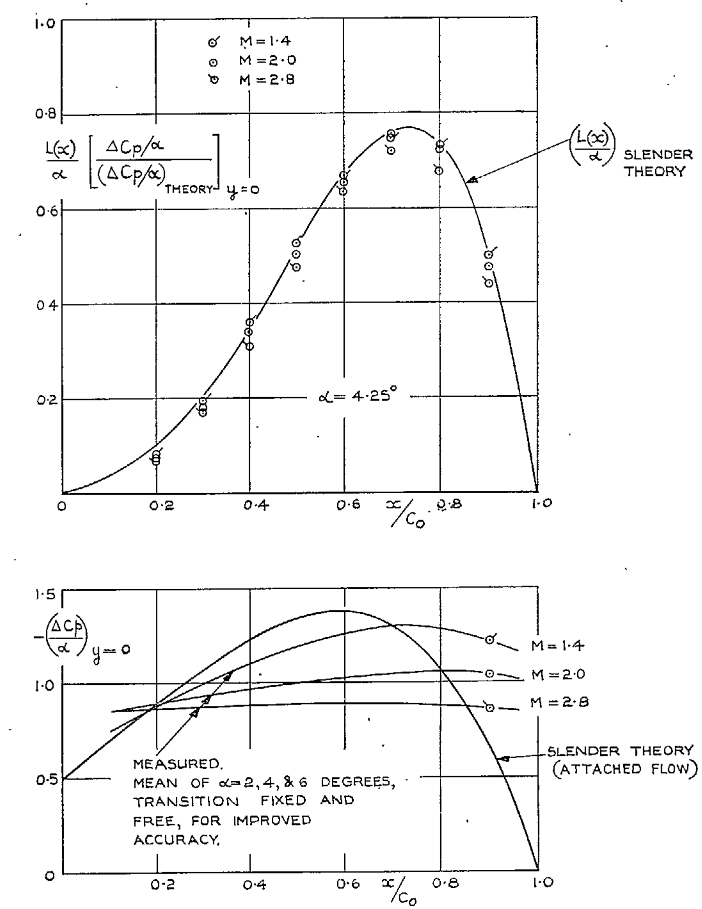

FIG. 22. Apparent collapse of cross-load distributions in terms of local load at centre-line.

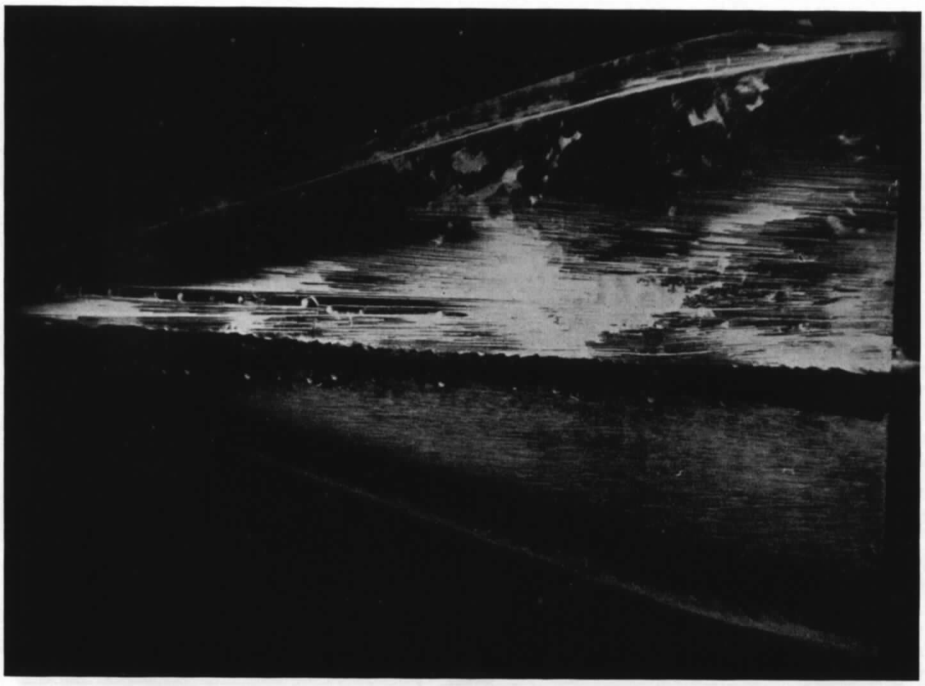

$M = 1{\cdot}4.$

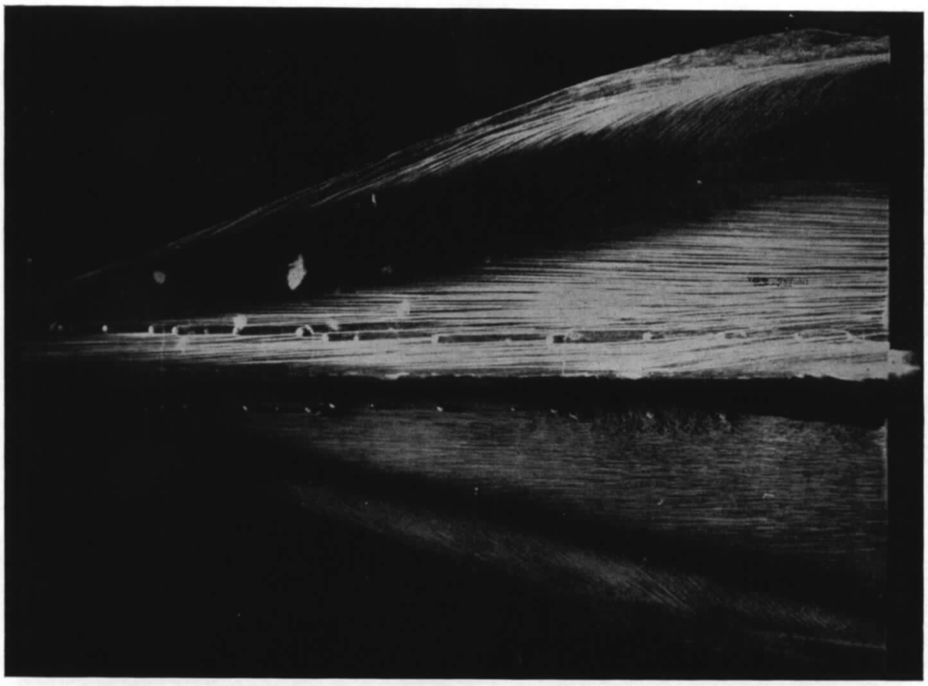

$M = 2{\cdot}0.$

FIG. 23. Oil-flow pictures at $\alpha = 6{\cdot}4°$.

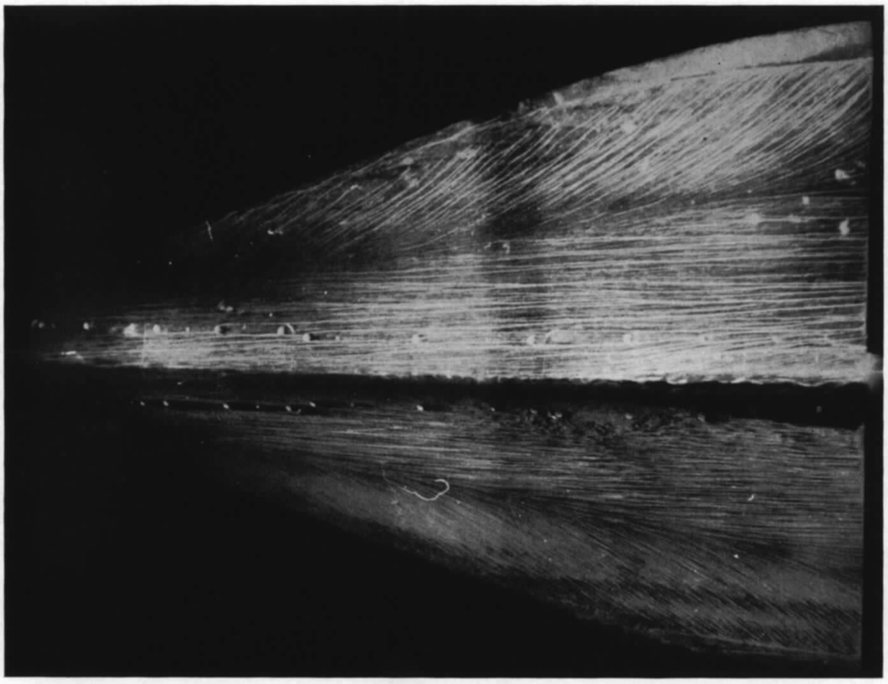

$M = 2{\cdot}4.$

$M = 2{\cdot}8.$

FIG. 23—*continued*. Oil-flow pictures at $\alpha = 6{\cdot}4°$.

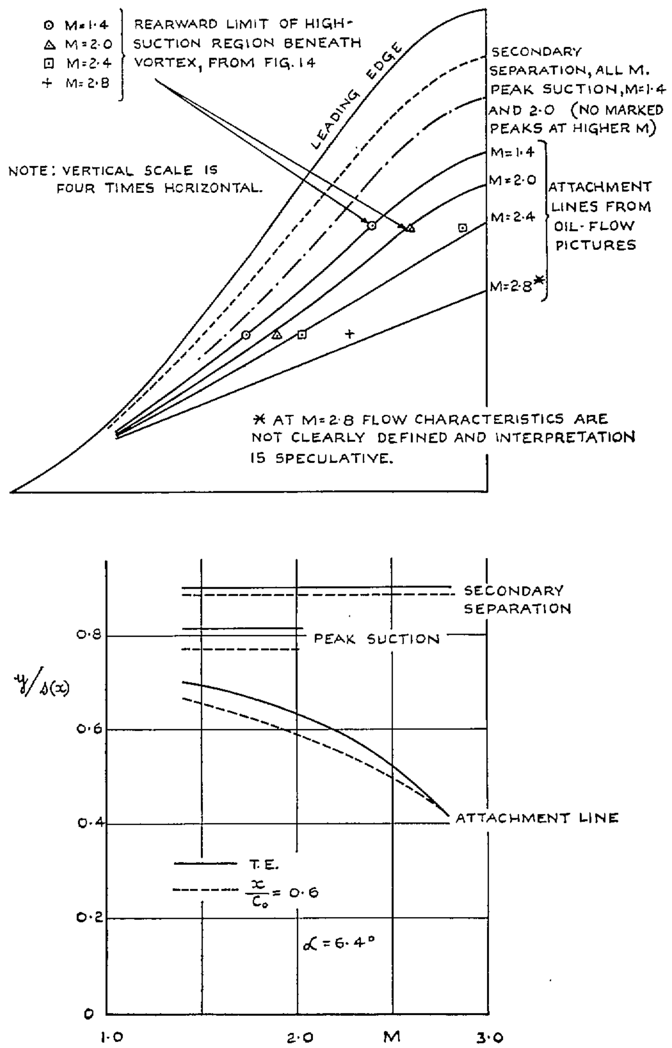

FIG. 24. Attachment lines, etc., at various Mach numbers, $\alpha = 6{\cdot}4°$.

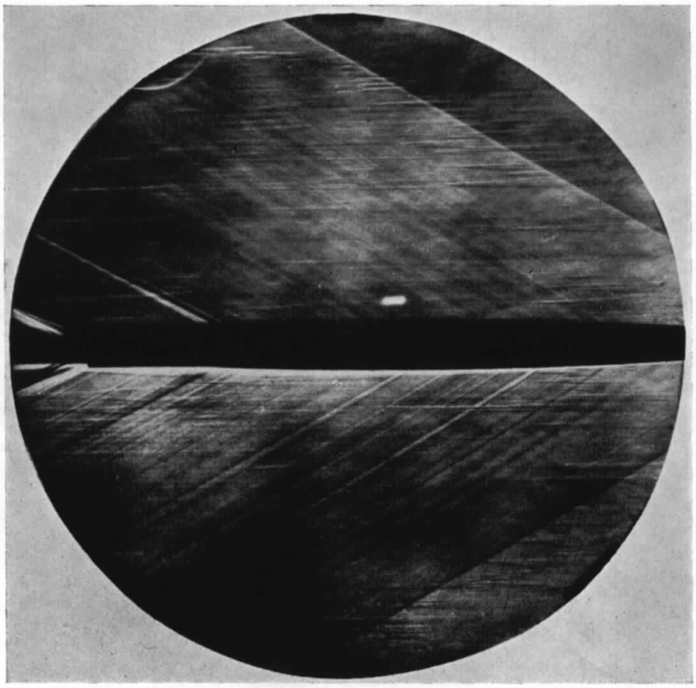

$M = 2 \cdot 0$.

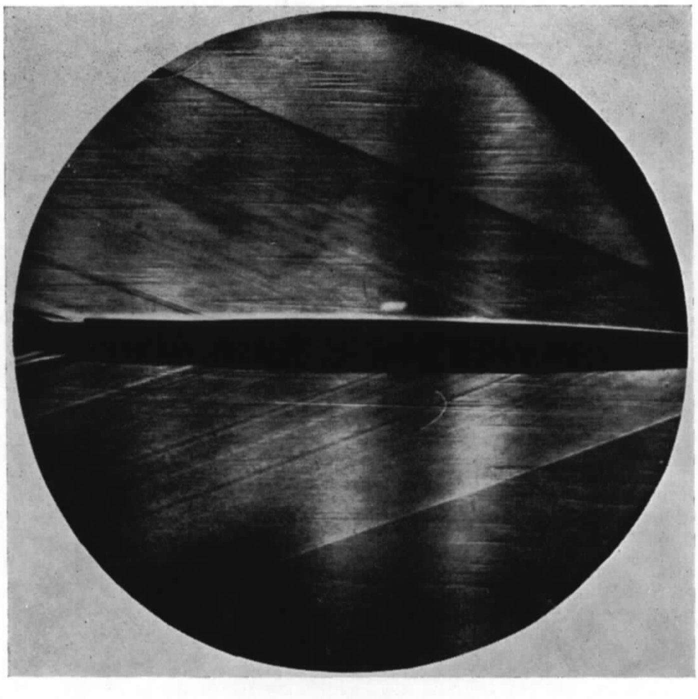

$M = 2 \cdot 8$.

FIG. 25. Schlieren pictures at zero incidence.

(89022) Wt. 65/1418 K.5 7/64 Hw.

Publications of the Aeronautical Research Council

ANNUAL TECHNICAL REPORTS OF THE AERONAUTICAL RESEARCH COUNCIL (BOUND VOLUMES)

1942 Vol. I. Aero and Hydrodynamics, Aerofoils, Airscrews, Engines. 75*s.* (post 2*s.* 9*d.*)
Vol. II. Noise, Parachutes, Stability and Control, Structures, Vibration, Wind Tunnels. 47*s.* 6*d.* (post 2*s.* 3*d.*)

1943 Vol. I. Aerodynamics, Aerofoils, Airscrews. 80*s.* (post 2*s.* 6*d.*)
Vol. II. Engines, Flutter, Materials, Parachutes, Performance, Stability and Control, Structures. 90*s.* (post 2*s.* 9*d.*)

1944 Vol. I. Aero and Hydrodynamics, Aerofoils, Aircraft, Airscrews, Controls. 84*s.* (post 3*s.*)
Vol. II. Flutter and Vibration, Materials, Miscellaneous, Navigation, Parachutes, Performance, Plates and Panels, Stability, Structures, Test Equipment, Wind Tunnels. 84*s.* (post 3*s.*)

1945 Vol. I. Aero and Hydrodynamics, Aerofoils. 130*s.* (post 3*s.* 6*d.*)
Vol. II. Aircraft, Airscrews, Controls. 130*s.* (post 3*s.* 6*d.*)
Vol. III. Flutter and Vibration, Instruments, Miscellaneous, Parachutes, Plates and Panels, Propulsion. 130*s.* (post 3*s.* 3*d.*)
Vol. IV. Stability, Structures, Wind Tunnels, Wind Tunnel Technique. 130*s.* (post 3*s.* 3*d.*)

1946 Vol. I. Accidents, Aerodynamics, Aerofoils and Hydrofoils. 168*s.* (post 3*s.* 9*d.*)
Vol. II. Airscrews, Cabin Cooling, Chemical Hazards, Controls, Flames, Flutter, Helicopters, Instruments and Instrumentation, Interference, Jets, Miscellaneous, Parachutes. 168*s.* (post 3*s.* 3*d.*)
Vol. III. Performance, Propulsion, Seaplanes, Stability, Structures, Wind Tunnels. 168*s.* (post 3*s.* 6*d.*)

1947 Vol. I. Aerodynamics, Aerofoils, Aircraft. 168*s.* (post 3*s.* 9*d.*)
Vol. II. Airscrews and Rotors, Controls, Flutter, Materials, Miscellaneous, Parachutes, Propulsion, Seaplanes, Stability, Structures, Take-off and Landing. 168*s.* (post 3*s.* 9*d.*)

1948 Vol. I. Aerodynamics, Aerofoils, Aircraft, Airscrews, Controls, Flutter and Vibration, Helicopters, Instruments, Propulsion, Seaplane, Stability, Structures, Wind Tunnels. 130*s.* (post 3*s.* 3*d.*)
Vol. II. Aerodynamics, Aerofoils, Aircraft, Airscrews, Controls, Flutter and Vibration, Helicopters, Instruments, Propulsion, Seaplane, Stability, Structures, Wind Tunnels. 110*s.* (post 3*s.* 3*d.*)

Special Volumes

Vol. I. Aero and Hydrodynamics, Aerofoils, Controls, Flutter, Kites, Parachutes, Performance, Propulsion, Stability. 126*s.* (post 3*s.*)
Vol. II. Aero and Hydrodynamics, Aerofoils, Airscrews, Controls, Flutter, Materials, Miscellaneous, Parachutes, Propulsion, Stability, Structures. 147*s.* (post 3*s.*)
Vol. III. Aero and Hydrodynamics, Aerofoils, Airscrews, Controls, Flutter, Kites, Miscellaneous, Parachutes, Propulsion, Seaplanes, Stability, Structures, Test Equipment. 189*s.* (post 3*s.* 9*d.*)

Reviews of the Aeronautical Research Council

1939–48 3*s.* (post 6*d.*) 1949–54 5*s.* (post 5*d.*)

Index to all Reports and Memoranda published in the Annual Technical Reports

1909–1947 R. & M. 2600 (out of print)

Indexes to the Reports and Memoranda of the Aeronautical Research Council

Between Nos. 2351–2449	R. & M. No. 2450	2*s.* (post 3*d.*)
Between Nos. 2451–2549	R. & M. No. 2550	2*s.* 6*d.* (post 3*d.*)
Between Nos. 2551–2649	R. & M. No. 2650	2*s.* 6*d.* (post 3*d.*)
Between Nos. 2651–2749	R. & M. No. 2750	2*s.* 6*d.* (post 3*d.*)
Between Nos. 2751–2849	R. & M. No. 2850	2*s.* 6*d.* (post 3*d.*)
Between Nos. 2851–2949	R. & M. No. 2950	3*s.* (post 3*d.*)
Between Nos. 2951–3049	R. & M. No. 3050	3*s.* 6*d.* (post 3*d.*)
Between Nos. 3051–3149	R. & M. No. 3150	3*s.* 6*d.* (post 3*d.*)

HER MAJESTY'S STATIONERY OFFICE

from the addresses overleaf

R. & M. No. 3361

Printed and published by
HER MAJESTY'S STATIONERY OFFICE

To be purchased from
York House, Kingsway, London W.C.2
423 Oxford Street, London W.1
13A Castle Street, Edinburgh 2
109 St. Mary Street, Cardiff
39 King Street, Manchester 2
50 Fairfax Street, Bristol 1
35 Smallbrook, Ringway, Birmingham 5
80 Chichester Street, Belfast 1
or through any bookseller

Printed in England

R. & M. No. 3361

S.O. Code No. 23-3361